

1 **Innovations in Primate Interneuron Repertoire**

2  
3 Fenna M. Krienen<sup>1,2</sup>, Melissa Goldman<sup>1,2</sup>, Qiangge Zhang<sup>2,3</sup>, Ricardo del Rosario<sup>2</sup>, Marta Florio<sup>1,2</sup>,  
4 Robert Machold<sup>4</sup>, Arpiar Saunders<sup>1,2</sup>, Kirsten Levandowski<sup>2,3</sup>, Heather Zaniewski<sup>2,3</sup>, Benjamin  
5 Schuman<sup>4</sup>, Carolyn Wu<sup>3</sup>, Alyssa Lutservitz<sup>1,2</sup>, Christopher D. Mullally<sup>1,2</sup>, Nora Reed<sup>1,2</sup>, Elizabeth  
6 Bien<sup>1,2</sup>, Laura Bortolin<sup>1,2</sup>, Marian Fernandez-Otero<sup>2,5</sup>, Jessica Lin<sup>2,5</sup>, Alec Wysoker<sup>2</sup>, James  
7 Nemesh<sup>2</sup>, David Kulp<sup>2</sup>, Monika Burns<sup>3</sup>, Victor Tkachev<sup>6</sup>, Richard Smith<sup>6,7</sup>, Christopher A.  
8 Walsh<sup>6,7</sup>, Jordane Dimidschstein<sup>2</sup>, Bernardo Rudy<sup>4,8</sup>, Leslie Kean<sup>6</sup>, Sabina Berretta<sup>5,9,10</sup>, Gord  
9 Fishell<sup>2,5</sup>, Guoping Feng<sup>2,3</sup>, Steven A. McCarroll<sup>1,2</sup>

10  
11 <sup>1</sup> Department of Genetics, Harvard Medical School, Boston, MA 02115

12 <sup>2</sup> Stanley Center for Psychiatric Research, Broad Institute of MIT and Harvard, Cambridge, MA  
13 02142, USA

14 <sup>3</sup> McGovern Institute for Brain Research, Department of Brain and Cognitive Sciences,  
15 Massachusetts Institute of Technology, Cambridge, Massachusetts, USA

16 <sup>4</sup> NYU Neuroscience Institute, Langone Medical Center, New York, New York 10016, USA.

17 <sup>5</sup> Program in Neuroscience, Harvard Medical School, Boston, MA 02215, USA

18 <sup>6</sup> Department of Pediatrics, Boston Children's Hospital, Boston, MA 02115

19 <sup>7</sup> Division of Genetics and Genomics, Boston Children's Hospital, Boston, MA 02115

20 <sup>8</sup> Department of Anesthesiology, Perioperative Care and Pain Medicine, New York University  
21 School of Medicine, New York, NY 10016

22  
23 <sup>9</sup> McLean Hospital, Belmont, MA 02478, USA

24 <sup>10</sup> Department of Psychiatry, Harvard Medical School, Boston, MA 02215, USA

25

26 **ABSTRACT**

27 Primates and rodents, which descended from a common ancestor more than 90 million years  
28 ago, exhibit profound differences in behavior and cognitive capacity. Modifications,  
29 specializations, and innovations to brain cell types may have occurred along each lineage. We  
30 used Drop-seq to profile RNA expression in more than 184,000 individual telencephalic  
31 interneurons from humans, macaques, marmosets, and mice. Conserved interneuron types  
32 varied significantly in abundance and RNA expression between mice and primates, but varied  
33 much more modestly among primates. In adult primates, the expression patterns of dozens of  
34 genes exhibited spatial expression gradients among neocortical interneurons, suggesting that  
35 adult neocortical interneurons are imprinted by their local cortical context. In addition, we found  
36 that an interneuron type previously associated with the mouse hippocampus—the “ivy cell”, which  
37 has neurogliaform characteristics—has become abundant across the neocortex of humans,  
38 macaques, and marmosets. The most striking innovation was subcortical: we identified an  
39 abundant striatal interneuron type in primates that had no molecularly homologous cell population  
40 in mouse striatum, cortex, thalamus, or hippocampus. These interneurons, which expressed a  
41 unique combination of transcription factors, receptors, and neuropeptides, including the  
42 neuropeptide *TAC3*, constituted almost 30% of striatal interneurons in marmosets and humans.  
43 Understanding how gene and cell-type attributes changed or persisted over the evolutionary  
44 divergence of primates and rodents will guide the choice of models for human brain disorders and  
45 mutations and help to identify the cellular substrates of expanded cognition in humans and other  
46 primates.

47

## 48 INTRODUCTION

49

50 Vertebrate brains contain many specialized brain structures, each with its own evolutionary  
51 history. For example, the six-layer neocortex arose in mammals around 200 million years ago<sup>1</sup>,  
52 whereas distinct basal ganglia nuclei were already present in the last common ancestor of  
53 vertebrates more than 500 million years ago<sup>2</sup>.

54

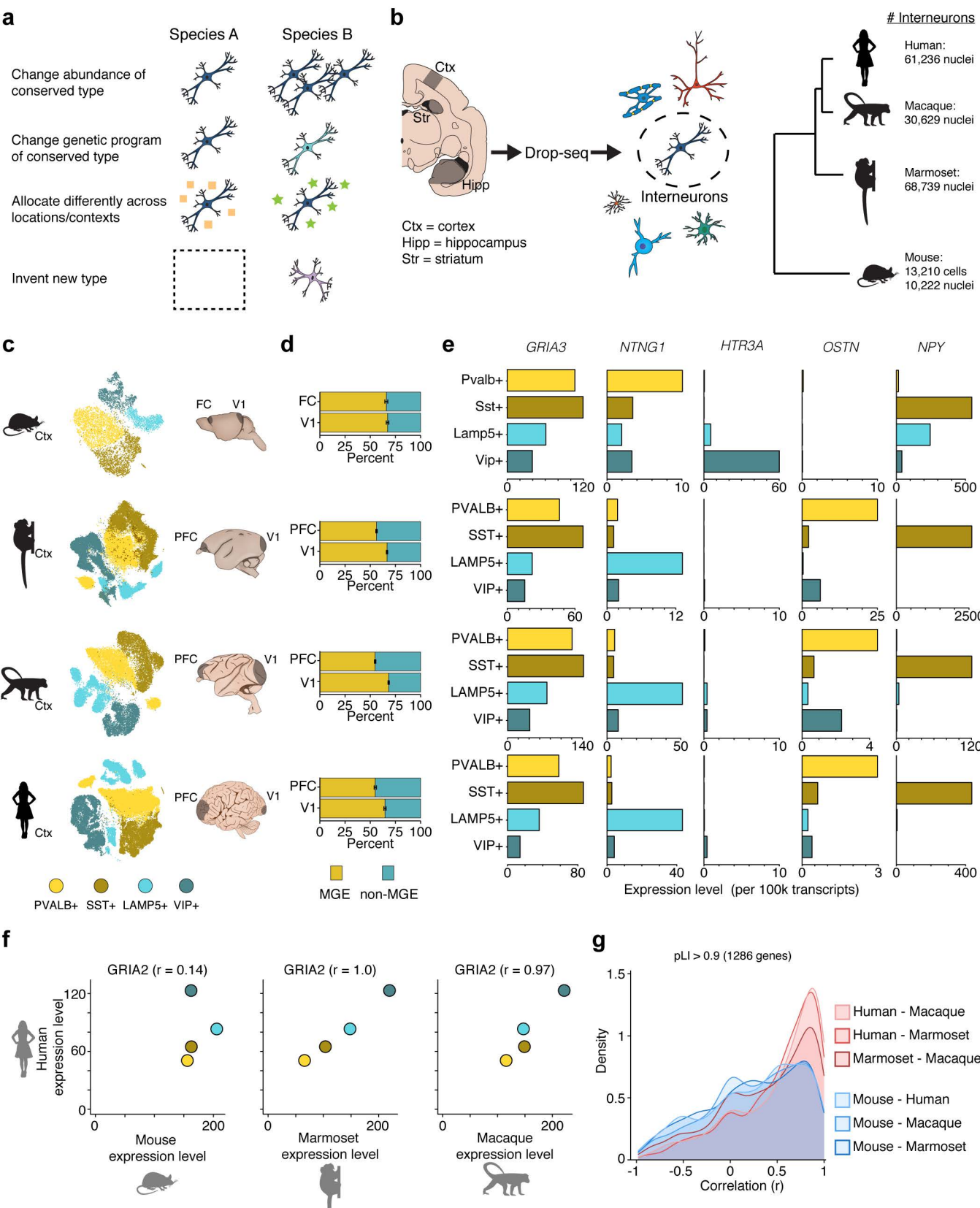
55 Brain structures, circuits, and cell types have acquired adaptations and new functions along  
56 specific evolutionary lineages. Numerous examples of modifications to specific cell types within  
57 larger conserved brain systems have been discovered, including hindbrain circuits that control  
58 species-specific courtship calls in frogs<sup>3</sup>, the evolution of trichromatic vision in primates<sup>4</sup>, and  
59 neurons that have converted from motor to sensory processing to produce a novel swimming  
60 behavior in sand crabs<sup>5</sup>. Evolution can modify brain structures through a wide range of  
61 mechanisms, including increasing or reducing production of cells of a given type, altering the  
62 molecular and cellular properties of shared cell types, reallocating or redeploying cell types to  
63 new locations in the brain, or inventing entirely new cell types (Fig. 1a).

64

65 Single-cell RNA sequencing, which systematically measures gene expression in thousands of  
66 individual cells, has recently enabled detailed comparisons of cell types and expression patterns  
67 between homologous brain structures separated by millions of years of evolution<sup>4,6,7</sup> (non-single  
68 cell approaches have also yielded important insights in this domain, e.g. <sup>8</sup>). For example, one  
69 recent study compared neocortical cells between humans and mice, identifying conserved and  
70 diverged features of many cell types<sup>7</sup>. It is not yet known which of the many differences between  
71 mouse and human brains are specific to humans, and which are shared among primates.

72

**Figure 1**



73

74 **Figure 1. Analysis of cortical interneurons in mouse, marmoset, macaque, and human.** **a,**  
75 Schematic showing possible modes of change in cellular assemblies across species. **b,**  
76 Schematic of experimental workflow and numbers of interneurons sampled in each species.  
77 Region abbreviations: Ctx = neocortex, Hipp = hippocampus, Str = striatum. **c,** t-distributed  
78 stochastic neighbor embedding (t-SNE) of cortical interneurons in each species. Cells are colored  
79 by membership in one of the four major neocortical classes: *SST+*, *PVALB+*, *VIP+*, or *LAMP5+*  
80 (dark brown or dark green cells represent the minority of cells that co-expressed *SST* and *PVALB*  
81 or *LAMP5* and *VIP*, respectively). **d,** The proportion of medial ganglionic eminence (MGE)-derived  
82 (*SST+* or *PVALB+*) and non-MGE-derived (*VIP+* or *LAMP5+*) types across two cortical regions  
83 (frontal/prefrontal cortex, PFC, and visual cortex, V1) for each species. Error bars represent 95%  
84 binomial confidence intervals. **e,** Examples of markers with different enrichment patterns across  
85 species (see also Extended Data Fig. 1b). Values are scaled expression levels (number of  
86 transcripts per 100k) for each of the four main cortical interneuron classes. **f,** Scaled expression  
87 levels (number of transcripts per 100k) for *GRIA2*, a gene encoding an AMPA receptor subunit,  
88 in human vs. mouse, marmoset, and macaque for the four major interneuron classes. Dots are  
89 colored as in (e). **g,** Density histograms showing correlation distribution of expressed genes  
90 between pairs of species (red = primate–primate pairs, blue = primate–mouse pairs). pLI =  
91 probability of loss of function intolerance.  
92

93 In this study, we compared interneurons, a major class of neurons present in all vertebrates, in  
94 mice and three primates: marmoset, macaque, and human, which span ~90 million years of  
95 evolutionary divergence (Fig. 1b). Interneurons contribute to local circuit assemblies and provide  
96 the main source of inhibition in neuronal circuits by releasing the inhibitory neurotransmitter  
97 GABA. Interneurons are born subcortically from progenitors that reside in transient proliferative  
98 zones called the ganglionic eminences, including the medial and caudal ganglionic eminences  
99 (MGE and CGE), and migrate to the neocortex and to subcortical structures during development<sup>9</sup>.  
100 Interneurons are particularly interesting for comparative analysis because they are  
101 morphologically and physiologically diverse within any one species, but major types are shared  
102 across the amniotes<sup>10</sup>. In mice, the same interneuron types recur across functionally distinct  
103 neocortical regions<sup>11,12</sup>. An understanding of interneurons' evolution in primates and rodents could  
104 guide the choice of models for studying how microcircuits and excitatory/inhibitory balance are  
105 affected in human brain disorders. Moreover, although the main developmental origins for

106 interneurons appear conserved, we still do not know how interneurons are qualitatively and  
107 quantitatively allotted to their destinations, nor the extent to which local cues shape interneuron  
108 gene expression in different species.

109

### 110 **Identifying interneurons in mice and primates**

111 We used Drop-seq<sup>13</sup>, a single-cell RNA sequencing technology, to measure RNA expression in  
112 nuclei of telencephalic brain cells (i.e., cells from brain regions including neocortex, hippocampus,  
113 and striatum) from adult animals of four species: mouse, common marmoset, rhesus macaque,  
114 and human. By applying unsupervised methods to the data from each individual species and from  
115 combinations of species, we classified transcriptionally distinct and similar groups of cells. We  
116 identified interneurons using canonical, conserved markers (e.g., *GAD1* and *GAD2*, which encode  
117 the glutamate decarboxylase required for synthesis of GABA) as well as class-specific molecular  
118 markers. In total, we sampled 68,739 telencephalic interneurons from marmoset, 61,236 from  
119 human, 30,629 from macaque, and 23,432 from mouse.

120

121 It was not previously known whether the broad classes of interneurons identified in mouse<sup>11,12,14</sup>  
122 also exist in all three primates, and if so, whether they could be delineated with the same set of  
123 markers. Across all four species, the same four genes (*SST*, *PVALB*, *VIP*, and *LAMP5*) exhibited  
124 mutually exclusive expression while together accounting for almost 100% of neocortical  
125 interneurons, suggesting that these markers stably delineate a core repertoire of interneuron  
126 types among rodents and primates (Fig. 1c; see also<sup>7</sup>).

127

### 128 **Interneuron abundances and local specialization in neocortex**

129 Within conserved brain structures, evolutionary changes in cell numbers or proportions can have  
130 profound functional consequences; such alterations appear to be major effectors of brain  
131 evolution<sup>5,15,16</sup>. Mammalian neocortex is patterned into functionally specialized fields, called

132 areas, that differ in cytoarchitecture, cell number, and connectivity. There is a fundamental  
133 distinction between primary sensory areas of the neocortex, which process visual, auditory and  
134 tactile information as part of well-defined hierarchies, and association areas such as prefrontal  
135 cortex, which perform higher-order functions. Primates, and particularly humans, have  
136 neocortices that are disproportionately enlarged relative to those of other mammals<sup>17</sup>. The  
137 accompanying changes in cellular composition are not well understood, although recent  
138 quantitative stereological methods have begun to relate cortical specialization to cell-type  
139 composition across the neocortex<sup>16</sup>.

140

141 In primates, but not mice, frontal association areas (FC/PFC) differed from primary visual cortex  
142 (V1) in the extent to which interneurons were derived from MGE as opposed to other eminences  
143 (Fig. 1d). In all four species, V1 contained similar proportions of MGE (marked by *SST* or *PVALB*)  
144 and non-MGE interneurons (marked by *VIP* or *LAMP5*): ~66% MGE and ~34% non-MGE. In  
145 primates, however, PFC harbored a significantly higher proportion of non-MGE interneurons  
146 (~55% MGE, ~45% non-MGE; Fig. 1c). Like PFC, association areas in temporal and parietal  
147 cortex contained proportionally more non-MGE-derived interneurons than V1 (Extended Data  
148 Fig. 1a). In primates, the upper neocortical layers have enlarged, particularly in association  
149 cortex<sup>18</sup>. Because MGE-derived interneurons preferentially populate deep layers<sup>19</sup>, the  
150 proportional increase in non-MGE-derived interneurons in primates is consistent with  
151 enlargement of upper-layer neocortical compartments and suggests greater recruitment of  
152 interneurons from the CGE to association cortex in primates.

153

#### 154 **Genetic programs within conserved interneuron types**

155 Homologous cell types can acquire species-specific functions through changes in gene  
156 expression<sup>9,16,17</sup>. To evaluate the extent to which gene-expression specializations distinguishing  
157 interneuron types are shared across species, we compared the expression level of each gene

158 across the four principal interneuron classes (*PVALB*<sup>+</sup>, *SST*<sup>+</sup>, *LAMP5*<sup>+</sup>, *VIP*<sup>+</sup>) within each  
159 species, and then compared these class-specific relative expression profiles across the species  
160 surveyed. (Comparing within and then across species corrects for species-specific [e.g.  
161 sequence-related] influences on mRNA sampling, as well as for latent technical variables that  
162 might distinguish brains from different species.) This analysis enabled identification of conserved  
163 gene expression patterns. For example, *GRIA3*, which encodes an AMPA receptor subunit, was  
164 expressed in similar patterns across the four classes (*SST*<sup>+</sup> > *PVALB*<sup>+</sup> > *ID2*<sup>+</sup> > *VIP*<sup>+</sup>) in all four  
165 species (Fig. 1e).

166

167 We first focused on genes that were selectively expressed at least one interneuron type (relative  
168 to the others) in at least one species (examples in Fig. 1e and Extended Data Fig. 1b). A clear  
169 pattern emerged: the great majority of human–mouse gene expression differences were shared  
170 among all three primates. For example, the neuropeptide Y (*NPY*) gene, a commonly used  
171 marker for specific interneurons, was expressed in both *SST*<sup>+</sup> and *LAMP5*<sup>+</sup> interneurons in  
172 mouse but was selectively expressed in *SST*<sup>+</sup> interneurons in marmoset, macaque, and humans.  
173 The netrin G1 (*NTNG1*) gene was, in mouse neocortex, selectively expressed in *PVALB*<sup>+</sup>  
174 interneurons; in primate neocortex, *NTNG1* was instead expressed by *LAMP5*<sup>+</sup> interneurons. In  
175 rare cases, a gene was enriched as a specific marker in one cell class in primates (e.g. *OSTN* in  
176 *PVALB*<sup>+</sup> interneurons) but not detected at all in mouse interneurons<sup>20</sup>, or vice versa (e.g., *HTR3A*,  
177 which encodes serotonin receptor 3a, see also<sup>7</sup>). Other examples included synuclein gamma  
178 (*Sncg*), the short transient receptor potential channel 3 (*Trpc3*), and the IQ motif containing  
179 GTPase activating protein 2 (*Iqgap2*), which were expressed specifically in certain classes of  
180 interneurons in mice, but were either widely expressed (*SNCG*) or enriched in a different  
181 population (*TRPC3*, *IQGAP2*) among neocortical interneurons from primates (Extended Data Fig.  
182 1b). Such cross-species expression variation has implications for choosing selective markers to  
183 define or characterize conserved cell types.



184

185 Far more genes were expressed in many or all neuronal types at quantitatively distinct levels. We  
186 know little about the extent to which the precise expression levels of such genes contribute to the  
187 specialized functions of neuronal types. However, understanding such relationships will be  
188 important for interpreting the significance of noncoding genetic variation in humans, as well as  
189 for selecting appropriate models for heterozygous mutations ascertained in human patients. A  
190 comparative lens can reveal the extent to which evolution has maintained a gene's quantitative  
191 expression level in different cell types relative to one another. To evaluate conservation at this  
192 level, we identified 4051 expressed genes that exhibited at least 1.5-fold expression variation  
193 among the four main interneuron classes, and calculated the cross-species correlation of each  
194 gene's expression measurements across those classes. Illustrating one of the main patterns  
195 revealed by this analysis, expression levels of *GRIA2*, a member of an AMPA receptor subunit  
196 family, exhibited relatively little variation ( $\pm 25\%$ ) among the four main interneuron classes in mice,  
197 but varied by 2–3-fold across the homologous interneuron types in primates, in a pattern (*VIP+* >  
198 *ID2+* and *SST+* > *PVALB+*) that was highly correlated across the three primates ( $r = 0.95\text{--}1.0$ ;  
199 Fig. 1f).

200

201 Genes that are dosage-sensitive in humans might have particularly strong evolutionary constraint  
202 on their expression levels. To evaluate this, we further focused on 1,286 genes that exhibit  
203 evidence of haploinsufficiency in humans as determined using pLI, a metric based on sequence  
204 variation across 60,706 human genomes that describes the probability that a given gene is  
205 intolerant of loss of function in human populations<sup>21</sup>. Relative expression of these human-  
206 haploinsufficient genes ( $pLI > 0.9$ ) in interneuron types appeared to be much more constrained  
207 among primates than in the primate–mouse comparisons (Fig. 1g). (A control analysis revealed  
208 that the subset of genes with low pLI scores ( $pLI < 0.1$ ) had correlation values around 0 for all  
209 species pairs, implying that genes that are tolerant of loss of function in humans are less

210 constrained in their expression levels.) This relationship suggests that even dosage-sensitive  
211 genes have undergone substantial evolutionary change in their quantitative expression levels,  
212 and that these levels are more similar among primates than between primates and mice.

213

214 We also compared pairs of cell types in each pair of species, evaluating the extent to which  
215 differential-expression relationships were conserved between species across genes that are  
216 meaningfully expressed (> 10 transcripts per 100,000) in interneurons (Extended Data Fig. 2).  
217 Such comparisons offered abundant evidence that the relative expression levels (between  
218 interneuron subtypes) of a vast number of mutually expressed genes have been conserved. The  
219 overall correlation of relative expression levels between cell-type pairs was stronger for  
220 comparisons between primates than for comparisons between mice and any of the primates  
221 (Extended Data Fig. 2c).

222

### 223 **Regional specialization of expression patterns within the neocortex**

224 To resolve types of interneurons at a finer scale, and to compare these types across species and  
225 brain regions, we used a computational approach, LIGER<sup>22</sup>, that aligns expression patterns  
226 across experiments and species (Extended Data Fig. 2), enabling us to compare gene expression  
227 programs within interneuron types across cortical regions (Fig. 2). In mouse, the expression  
228 programs of interneurons, in contrast to those of excitatory neurons, exhibit few differences across  
229 cortical locations<sup>11,12,23</sup>. In marmosets, each of 17 readily resolvable interneuron types was  
230 present in all seven cortical regions surveyed, confirming that, as in mouse, different cortical  
231 regions contain the same basic interneuron types (Fig. 2a). However, gene expression patterns  
232 for these conserved types differed across cortical regions. Across types, the median number of  
233 regionally differentially expressed genes (rDEGs, >3-fold difference) between PFC and V1 was  
234 55 (Fig. 2b), exceeding the number observed when comparing mouse frontal and posterior  
235 cortical areas using the same criteria (median = 12.5, see also<sup>11,12</sup>).

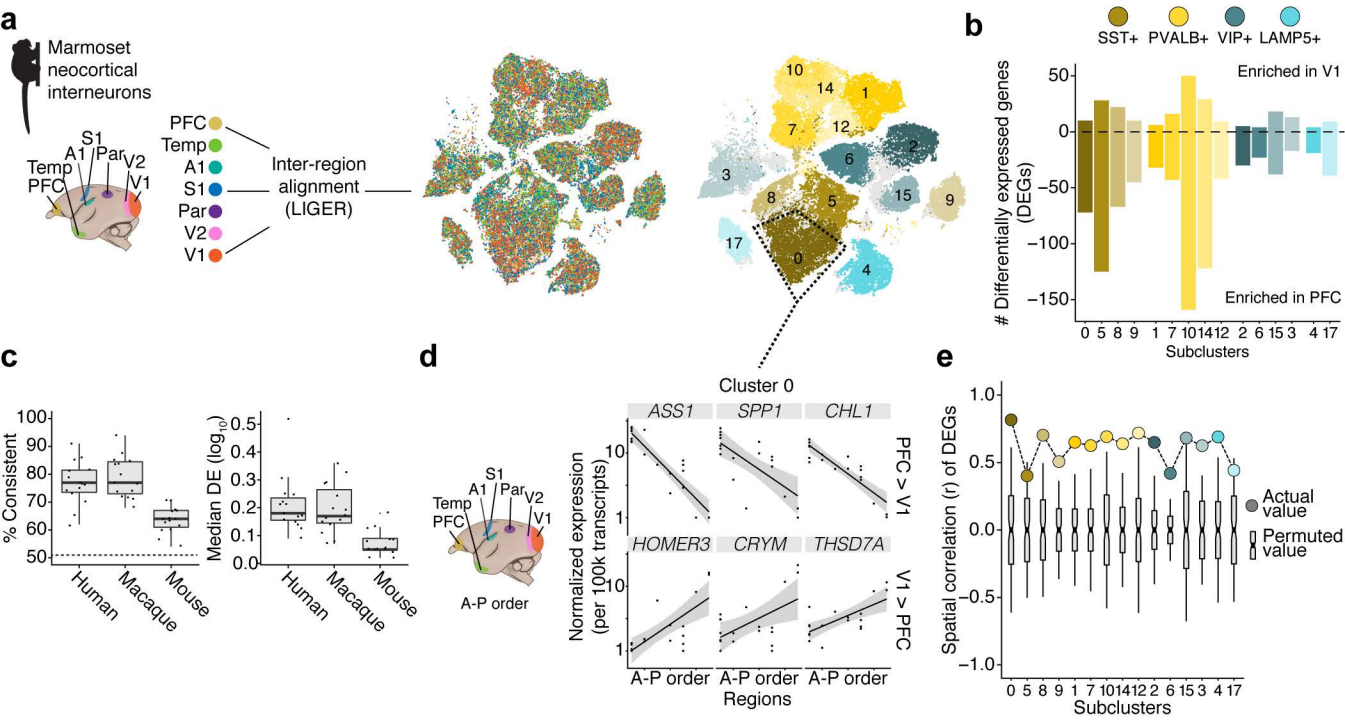
236

237 Although the number of rDEGs varied across clusters (Fig. 2b and Extended Data Fig. 3b), rDEGs  
238 identified for any one cluster or type tended to exhibit the same regional bias in the other clusters  
239 as well (Extended Data Fig. 3c,d). This suggests that most such differences reflect a common  
240 regional signature that is shared by diverse interneurons, rather than being specific to particular  
241 interneuron types. This regional bias did not extend to astrocytes (Extended Data Fig. 3e). The  
242 specific rDEGs defined in marmosets exhibited shared patterns of regional bias in interneurons  
243 in the other species: genes that were enriched in PFC vs V1 in marmoset were more likely to be  
244 more highly expressed in PFC than in V1 in the other three species, with greater probability and  
245 magnitude of difference in humans and macaques than in mice (Fig. 2c). These results suggest  
246 that interneurons acquire region-specific components of their molecular identities (see also<sup>24,25</sup>),  
247 and that these details are shared across species and most strongly among close relatives.

248

249

Figure 2



250 **Figure 2. Comparing cortical interneurons within and across species. a**, Integrative analysis  
251 of seven neocortical regions in marmoset using LIGER. t-SNE plots show resultant clusters with  
252 cells colored by cortical region of origin (left) and by cluster assignment (right). **b**, Histogram of  
253 the number of regionally differentially expressed genes (rDEGs) (>3-fold expression difference)  
254 between prefrontal (PFC) and primary visual cortex (V1) in each cell type (cluster) for which there  
255 were at least 50 cells per region. **c**, The rDEGs in marmoset (PFC, V1) tended to have the same  
256 regional differences in the other three species (left, percent of genes consistent with marmoset  
257 pattern; dashed line represents chance), with greater differential expression in humans and  
258 macaques than in mice (right). Dots represent rDEGs from each marmoset cluster; values were  
259 calculated from the cluster in the other species that had the most DE genes in common with that  
260 marmoset cluster. **d**, Normalized expression of rDEGs (identified between PFC and V1) across  
261 all seven neocortical regions in marmosets. X-axis arranged by anterior–posterior position of  
262 neocortical region. Plot shows the top three differentially expressed genes for the cluster outlined  
263 in **a** for each contrast (PFC>V1, V1>PFC). Dots are individual replicates within each region. **e**,  
264 Colored dots show averaged spatial correlations across rDEGs identified in each cluster when  
265 regions (n = 5, excluding PFC and V1) are arranged in anterior–posterior order. Gray boxplots  
266 show averaged correlations of the same rDEGs in each cluster when computed using permuted  
267 region orderings (n=120 possible orderings).  
268

269 Spatial patterns of gene expression, including macro-scale gradients and the distinction between  
270 primary and higher-order neocortical areas, configure the layout of neocortical areas during  
271 development<sup>26,27</sup> and persist into adulthood<sup>28</sup>. Gradients may contribute to excitatory neuron  
272 diversity<sup>29</sup>. Unlike excitatory neurons, which are born just below the neocortical areas in which  
273 they ultimately reside, neocortical interneurons are born subcortically and migrate into the  
274 neocortex post-mitotically; little is known about whether individual interneurons acquire  
275 information or specializations reflecting their ultimate areal locations within the neocortex. To  
276 explore this question, we investigated whether the expression of rDEGs identified in comparisons  
277 of PFC and V1 also varied across other neocortical regions. This analysis revealed a spatial logic:  
278 rDEG expression correlated strongly with anterior–posterior location (Fig. 2d); a control analysis  
279 in which region order was permuted yielded correlations distributed around zero (Fig. 2e). This  
280 anterior–posterior gradient is also correlated with, and might well reflect, the more complex  
281 patterns associated with the distinction between primary and higher-order neocortical areas<sup>30,31</sup>;  
282 for example, a number of genes had expression levels in parietal association cortex that were

283 more similar to those in temporal and prefrontal cortex than those in the sensory areas more  
284 proximal to it. (Definitively parsing the overlapping effects of anterior-posterior, sensory-  
285 association, and other topographies would require a comprehensive sampling of neocortical  
286 areas.) Together, these results suggest that neocortical interneurons intrinsically detect and  
287 encode some aspect of their ultimate spatial position.

288

### 289 **Re-allocation of a shared interneuron type across brain structures**

290 The main classes (*PVALB*, *SST*, *VIP*, *LAMP5*) of neocortical interneurons each contain many  
291 types<sup>32</sup>, and our analysis of the mouse and marmoset cortical interneurons (using LIGER)  
292 identified at least 15 transcriptionally distinct types (Extended Data Fig. 2b) with clear cross-  
293 species homologies in their global patterns of gene expression (Extended Data Fig. 4). These  
294 analyses affirm findings that homologous, molecularly-defined interneuron types can be identified  
295 across species spanning vast evolutionary distances, including reptiles, mice, and humans<sup>7,33</sup>.  
296 We have not attempted a definitive taxonomic classification here because we anticipate that  
297 improvements in single-cell technology and deeper ascertainment of neurons will further refine  
298 these categories.

299

300 The broad sharing of interneuron types, though, included notable differences. Notably, marmoset  
301 neocortex contained a substantial population of *LAMP5*+ cells that co-expressed *LHX6* (Fig. 3a).  
302 The existence of these interneurons in the neocortex raised intriguing questions because *LHX6*,  
303 a transcription factor, participates in cell fate determination of MGE types, whereas *LAMP5*+  
304 neocortical interneurons come from the CGE<sup>34</sup>. In mouse, neocortical *Lamp5*+ interneurons  
305 consist of neurogliaform and single-bouquet types, which are the most numerous type of Layer 1  
306 neuron and have distinct morphological, neurochemical, and connectivity properties<sup>9</sup>. Analysis by  
307 smFISH revealed that the spatial distribution of primate *LAMP5*+/*LHX6*+ neurons was distinct  
308 from that of *LAMP5*+/*LHX6*- neurons, with the former tending to reside within the deep cortical

309 layers (Fig. 3b). The proportion of interneurons that were *LAMP5+/LHX6+* was 10-fold higher in  
310 marmoset, macaque, and human cortex than in mouse cortex, in all cortical regions analyzed  
311 (Fig. 3c). Thus, this cell type, recently reported to be much more abundant in human temporal  
312 lobe than in mouse primary visual cortex<sup>7</sup>, appears to have expanded throughout the neocortex  
313 in an ancestor of diverse primates.

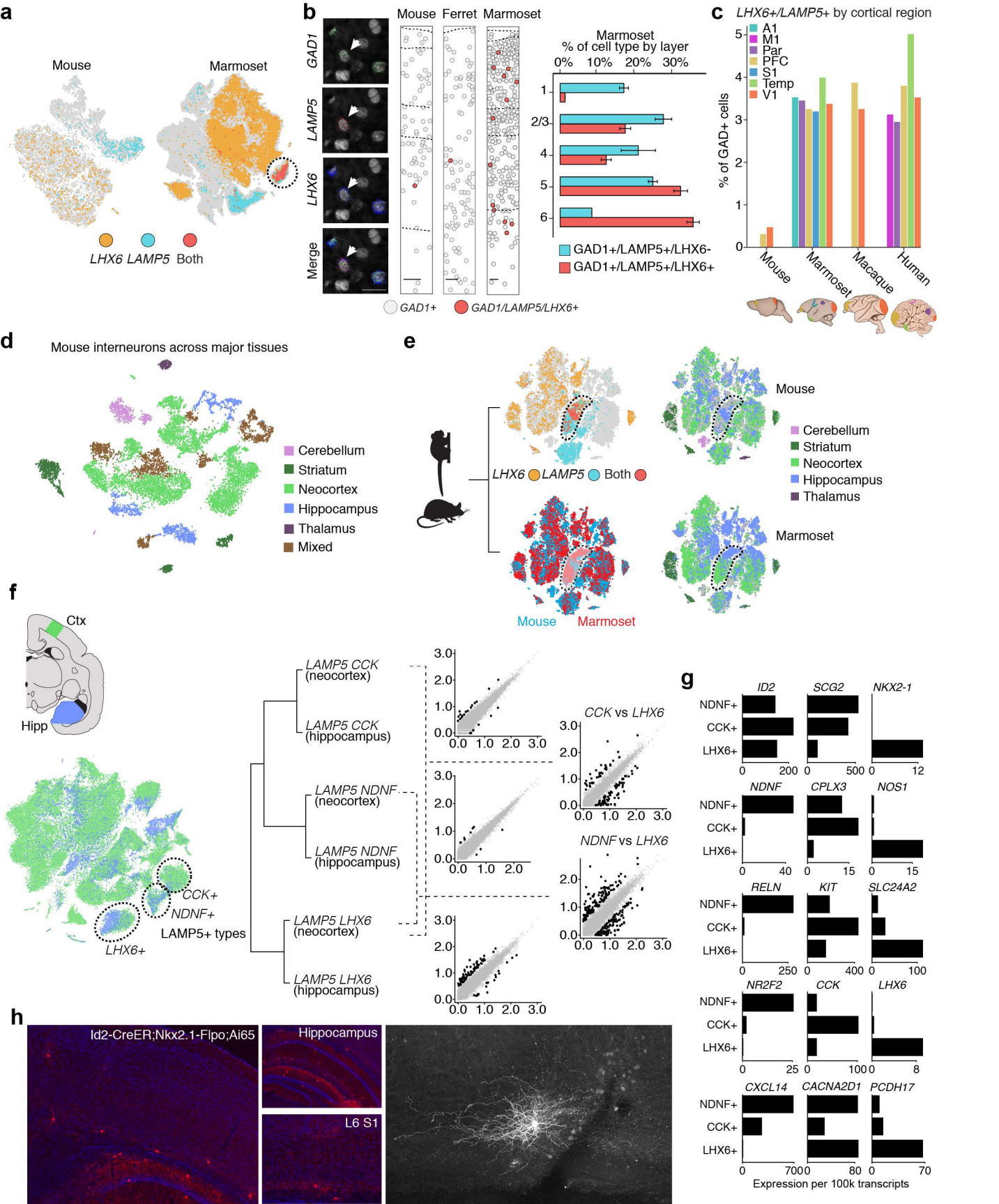
314

315 The *LAMP5/LHX6+* neurons could represent an innovation of primates or an ancestral condition  
316 lost by laboratory mice. The ferret, as a carnivore, serves as an outgroup relative to mice and  
317 primates. Analysis by smFISH for *LAMP5*, *LHX6*, and *GAD1* in ferret neocortex showed that, like  
318 mice, ferrets lacked a large deep layer *LAMP5+/LHX6+* interneuron population, suggesting that  
319 the expansion of *LAMP5+/LHX6+* interneurons is a primate innovation (Fig. 3b).

320

321 To better appreciate the developmental and evolutionary origins of *LAMP5+/LHX6+* interneurons,  
322 we sought clues from other brain areas. Progenitors in the ganglionic eminences give rise to  
323 interneurons that migrate to the neocortex, striatum, hippocampus, and other subcortical  
324 structures. Comparing the expression profile of the primate cortical *LAMP5+/LHX6+* population  
325 to expression profiles of 17,952 interneurons sampled from eight major structures of the mouse  
326 brain<sup>12</sup> revealed that primate cortical *LAMP5+/LHX6+* cells most closely resembled  
327 *Lamp5+/Lhx6+* interneurons in the mouse hippocampus (Fig. 3d,e). Although neurogliaform

328





329 **Figure 3. Cortical *LHX6*+/*LAMP5*+ interneurons are more numerous in primates and are**  
330 **molecularly similar to conserved hippocampal interneurons.**

331 **a**, Cells expressing *LHX6*, *LAMP5*, or both are plotted on t-SNEs from mouse and marmoset  
332 neocortical data. **b**, (left) Single molecule fluorescence *in situ* hybridization (smFISH) in marmoset  
333 neocortex showing an example of an *LHX6*+/*LAMP5*+/*GAD1*+ cell. (right) Quantification by layer  
334 of *LAMP5*+/*LHX6*-/*GAD1*+ cells (blue) and *LAMP5*+/*LHX6*+/*GAD1*+ cells (red) in marmoset  
335 neocortex. **c**, Abundances of *LHX6*+/*LAMP5*+ cells, expressed as proportions of *GAD1*+  
336 interneurons sampled by Drop-seq, in marmoset, macaque, and human. Each sampled  
337 neocortical region is plotted separately. **d**, Mouse interneurons across major brain structures  
338 from <sup>12</sup>. Clusters are colored based on their dominant region of origin. **e**, (left, top) Integrative  
339 cross-species analysis (using LIGER) of marmoset neocortical, hippocampal, and striatal  
340 interneurons and mouse interneurons from (**d**). (left, bottom) The same t-SNE, colored to show  
341 cells expressing *LHX6*, *LAMP5*, or both genes. Cluster outlined in t-SNE contains cells that  
342 express both *LAMP5* and *LHX6*. (right) The same t-SNE, colored for each species separately by  
343 cell region of origin. **f**, (left) Clustering of marmoset neocortex and hippocampal interneurons.  
344 (right) Hierarchical clustering of *LAMP5*+ subtypes, separated by region (neocortex and  
345 hippocampus). Scatter plots of relative gene expression in pairs of subtypes ( $\log_{10}$ ). **g**, Scaled,  
346 normalized expression of select gene markers that distinguish the three main *LAMP5*+ types. **h**,  
347 To identify this population in mouse, and to determine whether the same *Nkx2.1* lineage gives  
348 rise to such cells in hippocampus and neocortex, *Id2-CreER*; *Nkx2.1-Flpo*; *Ai65* animals were  
349 examined. (left) Overview including neocortex and hippocampus. (middle, top) Hippocampus was  
350 abundantly labeled. (middle, bottom) In neocortex, labeling was extremely sparse and mostly  
351 restricted to Layer 6. Labeled cells could be found rarely in L2/3, but not at all in L1. (right) A  
352 biocytin-filled mouse *Id2*;*Nkx2.1* interneuron in neocortical layer 6.

353

354 interneurons in the neocortex are thought to derive solely from the CGE, mouse hippocampal  
355 *Lamp5*+/*Lhx6*+ interneurons arise from the MGE; such neurons comprise the closely related ivy  
356 and neurogliaform subtypes, the most numerous hippocampal *Nos1*+ interneurons<sup>35</sup>.

357

358 To directly evaluate the similarity of the *LAMP5*+/*LHX6*+ populations in hippocampus and  
359 neocortex, we analyzed marmoset neocortical and hippocampal interneurons together (Fig. 3f).

360 The neocortical and hippocampal *LAMP5*+/*LHX6*+ populations formed a common cluster,  
361 indicating that they were more similar to each other than to the other two *LAMP5*+ neocortical  
362 subtypes, which did not express *LHX6* (Fig. 3f,g). Notably marmoset hippocampal and neocortical  
363 *LAMP5*+/*LHX6*+ populations expressed *NKX2-1* (Fig. 3g), which in mouse is obligately  
364 downregulated in MGE-derived interneurons destined for the neocortex<sup>36</sup> but persists in some

365 human cortical interneurons<sup>37</sup>. Fate mapping of interneurons identified by *Id2/Nkx2-1* in mice  
366 confirmed that the cortical and hippocampal populations arose from a common (MGE) origin (Fig.  
367 3h).

368  
369 Primates might have evolved customized allocation for these *LAMP5+/LHX6+* cells from the MGE  
370 to neocortex specifically or could have simply expanded the generation of these cells for all brain  
371 structures, for example by expanding their progenitor pool. To evaluate these possibilities, we  
372 asked whether the *LAMP5+/LHX6+* population has also increased in primate hippocampus.  
373 smFISH analyses in marmoset and mouse indicated that *LAMP5+/LHX6+* neurons populate  
374 the same hippocampal layers in the CA1/CA2 region (Extended Data Fig. 5, see also<sup>38</sup>). Thus,  
375 the ten-fold expansion of *LAMP5+/LHX6+* neurons in primates appears selective to the neocortex  
376 and is likely to represent differentially customized allocation (potentially via different rates or cues  
377 for migration, or via different rates of cell death) between neocortex and hippocampus relative to  
378 mice. Intriguingly, the *LAMP5+/LHX6+* cells are distinct from, but molecularly most closely related  
379 to, recently described *LAMP5+* cells that have acquired a distinct “rosehip” morphology and  
380 distinct physiological properties in human neocortex relative to their molecularly homologous cell  
381 population in mouse cortex<sup>7,39</sup>.

382

### 383 **A novel molecular interneuron type in primate striatum**

384 Although the neocortex has greatly expanded and specialized in the primate lineage<sup>18,40,41</sup>, the  
385 basal ganglia are deeply conserved collections of subcortical nuclei – so much so that the  
386 lamprey, which shared a last common ancestor with mammals more than 500 million years ago,  
387 retains nuclei, circuitry, and basic cell types homologous to those observed in mice<sup>2</sup>. Therefore,  
388 we expected that interneuron types in the striatum (the largest part of the basal ganglia) would be  
389 highly conserved between primates and mice. To our surprise, marmoset striatum revealed, in  
390 addition to all the major classes of striatal interneurons found in mice<sup>12,42</sup>, a transcriptionally

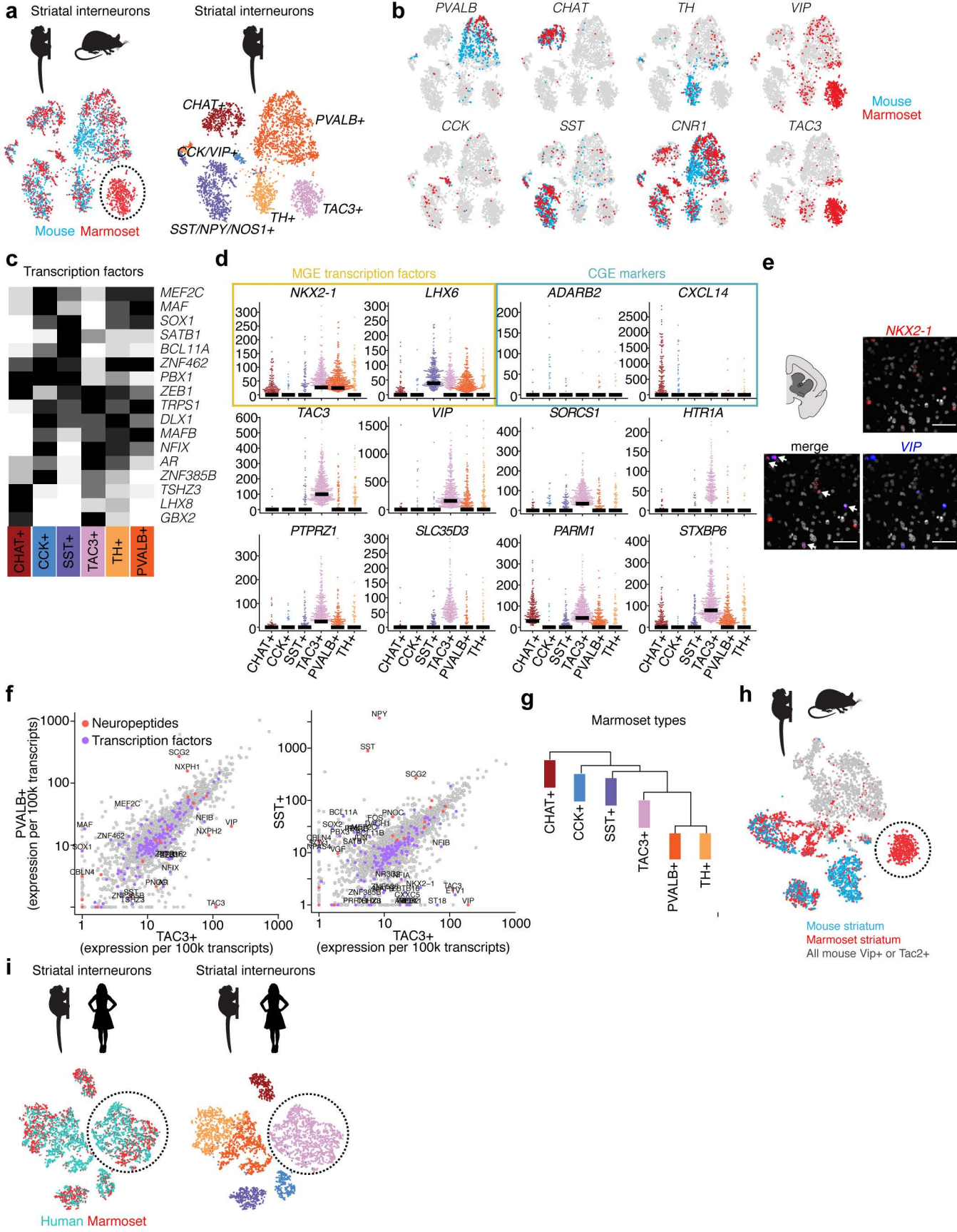
391 distinct type that expressed *VIP* and *TAC3*. This subtype did not appear to have a molecularly  
392 homologous population among mouse striatal interneurons (Fig. 4a-b). Because *VIP* is also  
393 sparsely expressed in other marmoset striatal interneuron types [Fig. 4b], we hereafter refer to  
394 the population as *TAC3+*. The *TAC3+* interneuron population was present in male and female  
395 marmosets and in multiple striatal nuclei, including the caudate nucleus, putamen, and nucleus  
396 accumbens. Surprisingly, it constituted ~30% of all interneurons in the striatum.

397

398 *TAC3+* interneurons expressed unique combinations of transcription factors, neuropeptides,  
399 transporters, and receptors that were not observed in other interneuron subtypes in marmosets  
400 (or in any subtype in mice) (Fig. 4c–f). These included genes encoding the androgen receptor  
401 (*AR*), serotonin receptor 1A (*HTR1A*), and sugar transporter *SLC35D3*.

402

403



404 **Figure 4. A primate striatal interneuron type not observed in mouse.** **a**, Integrative cross-  
405 species alignment (using LIGER) of marmoset and mouse striatal interneurons. **b**, Cells  
406 expressing markers for each interneuron cluster plotted for marmoset (red) and mouse (blue). **c**,  
407 Heat map of expressed transcription factors in marmoset for each striatal subtype. Each gene is  
408 scaled to its maximum value across types (black = max). **d**, Beeswarm plots showing additional  
409 markers that distinguish *TAC3+* interneurons from other interneuron types in marmoset, including  
410 MGE transcription factors (shaded yellow) and CGE markers (shaded blue). Dots are individual  
411 cells; bars indicate median expression. **e**, smFISH for *VIP* and *NKX2-1* in marmoset striatum.  
412 Cells that co-express both genes identified by arrows. **f**, Scatterplots showing gene expression  
413 ( $\log_{10}$ ) between *TAC3+* and *PVALB+* or *TAC3+* and *SST+* populations. Differentially expressed  
414 (> 3-fold difference) neuropeptides and transcription factors are labeled. **g**, Hierarchical clustering  
415 of all expressed genes within marmoset striatal subtypes. **h**, The analysis in (**a**) repeated, but  
416 additionally including all mouse extra-striatal interneurons from <sup>12</sup>. For display, the t-SNE shows  
417 marmoset striatal interneurons (red), mouse striatal interneurons (blue), and any extra-striatal  
418 mouse interneuron that expressed *Vip* or *Tac2* in the Saunders et al. <sup>12</sup> dataset (gray). Circled  
419 cells indicate marmoset *TAC3+* population. **i**, LIGER analysis pooling marmoset striatal  
420 interneurons with caudate interneurons isolated from human postmortem donors (n=2). Circled  
421 cluster indicates aligned marmoset and human *TAC3+* populations.  
422

423 The genes expressed by this novel population of striatal interneurons could provide hints about  
424 their developmental origins. Although *Vip* and *Tac2* (the mouse homologue of *TAC3*) are  
425 neuropeptide genes associated with CGE origin in mouse<sup>9</sup>, the marmoset *TAC3+* population  
426 expressed the MGE-associated transcription factors *LHX6* and *NKX2-1* (Fig. 4d). Because  
427 transcription factor and neuropeptide expression offered divergent clues, we used the entire  
428 genome-wide expression pattern to identify the interneurons most similar to the *TAC3+*  
429 interneurons. Hierarchical clustering situated the *TAC3+* population between the *SST+* and the  
430 *TH+* and *PVALB+* populations, all of which are MGE-derived (Fig. 4g). This suggests that despite  
431 expressing some CGE-associated neuropeptides, the *TAC3+* cells are more similar to striatal  
432 MGE-derived types than CGE-derived types.

433

434 To evaluate the possibility that a population of cells homologous to the *TAC3+* marmoset striatal  
435 interneurons might reside elsewhere in the mouse brain, as in the case of *LAMP5+/LHX6+*  
436 neocortical interneurons, we jointly analyzed the RNA expression profiles of marmoset striatal

437 interneurons and all interneurons from eight regions of the mouse brain (from <sup>12</sup>). The marmoset  
438 *TAC3+* population still formed its own cluster, suggesting that no homologous cell population  
439 existed in any of the mouse brain regions sampled (Fig. 4h). We also confirmed, by single-nucleus  
440 RNA sequencing, that no such population is present in ferret striatum, consistent with the  
441 interpretation that this cell population was introduced in the lineage leading to primates rather  
442 than being lost in mice.

443

444 The *TAC3+* interneuron population appeared to be shared between marmosets and humans:  
445 comparing marmoset striatal interneurons to interneurons obtained from the caudate nucleus from  
446 adult human postmortem donors identified a human striatal interneuron population with a  
447 homologous pattern of gene expression (Fig. 4i and Extended Data Fig. 6). The genes that were  
448 differentially expressed in marmoset between the *TAC3+* population and other striatal interneuron  
449 types also tended to be differentially expressed in the corresponding comparisons in human  
450 (Extended Data Fig. 6c). The *TAC3+* population constituted 38% of the interneurons sampled in  
451 human striatum.

452

453 The abundance of the novel, *TAC3+* interneuron population raised the question of whether it had  
454 replaced, or added to, conserved interneuron populations. The primates exhibited expanded  
455 representation of interneurons in the striatum overall: while interneurons were 4.1% of all striatal  
456 neurons in mice, they were 13.1% of all striatal neurons in marmosets and 10.8% in humans,  
457 consistent with stereological estimates of higher interneuron proportions in primate striatum<sup>43</sup>.  
458 Thus, compared to mice, primate striatum has more than doubled the proportion of interneurons,  
459 including an interneuron type with no clear homolog in mice.

460

461

462 **DISCUSSION**

463

464 “Cell types” have been defined as collections of cells that change together over the course  
465 evolution<sup>44,45</sup>. In this study, we found that although most of the major molecularly defined types of  
466 cortical interneurons are conserved across mice, humans, marmosets, and macaques, these  
467 interneurons nonetheless have undergone surprising levels of evolutionary change in the genes  
468 they express and the relative levels at which they express pan-neuronal genes. The significance  
469 of these changes for the detailed physiological and connectivity properties of interneurons will be  
470 important to understand<sup>46</sup>.

471

472 We found that the primate striatum contains an abundant interneuron type that has no  
473 homologous cell population in mice. These TAC3+ interneurons constituted 30% of interneurons  
474 in human and marmoset striatum, and expressed a suite of transcription factors and  
475 neuropeptides that distinguished them from other striatal interneurons. This innovation in primate  
476 striatum was accompanied by a broader expansion in the numbers of interneurons that doubled  
477 their representation as a fraction of all striatal neurons. These observations raise questions about  
478 how expanded numbers and types of interneurons have changed the functions of striatal  
479 microcircuits and their roles within the larger cortico-striatal circuits that contribute to primate  
480 cognition and potentially to neuropsychiatric disorders<sup>47</sup>.

481

482 We found that an interneuron type that is abundant in the mouse hippocampus—the ivy cell, which  
483 has properties similar to neurogliaform cells and is defined by co-expression of *Lamp5* and  
484 *Lhx6*<sup>35</sup>—has expanded throughout the neocortex in primates. Primates have retained ivy cells in  
485 the hippocampus but appear to have also greatly upregulated the production of these cells,  
486 increased their recruitment to the neocortex, and expanded their distribution throughout  
487 neocortical areas and layers. Other neurogliaform cell types in mouse neocortex are preferentially

488 found in upper layers and signal by volume transmission, the diffuse release of the inhibitory  
489 neurotransmitter GABA in the absence of conventional synapses<sup>48</sup>. Given that these cells were  
490 proportionally most numerous in the deep layers of the primate neocortex, one possibility is that  
491 in primates, these cells now contribute diffuse inhibitory signaling in new neocortical contexts.

492

493 The qualitative and quantitative deployment of gene expression across conserved interneuron  
494 types indicated that, even for genes that are pan-neuronally expressed, evolution has strongly  
495 constrained quantitative gene expression levels on evolutionary time scales, although substantial  
496 differences in gene expression and cellular proportions still clearly distinguish primates from mice.

497

498 Efforts to model the effects of specific genes and mutations on human brain function and illness  
499 could be facilitated by systematic data sets that reveal the extent to which each gene's cell-type–  
500 specific pattern of expression is shared by humans with each other species (e.g., <sup>8</sup>). We hope  
501 that the data from the experiments reported here will inform the design and interpretation of such  
502 studies. Accordingly, we have developed a simple, web-based data resource to enable cross-  
503 species comparisons of interneurons (<http://interneuron.mccarrolllab.org/>).

504

505 Our results reveal the ways in which the cellular and molecular repertoires of mouse and primate  
506 neurons have adapted over time. These evolutionary paths likely involved diverse developmental  
507 mechanisms, including alteration of neurogenesis rates, the creation of novel migratory pathways,  
508 and changes in gene regulation. Their effects on circuitry, cytoarchitecture, and physiology will  
509 be important and interesting to understand.

510

511 The innovations among interneurons are notable because the single-cell expression studies of  
512 tetrapod species performed to date – in lizards, turtles, mice, and primates – had suggested that



513 the known interneuron types are conserved across a broad taxonomic range. In this study,  
514 however, we identified surprising variation in interneurons within and across species, which was  
515 discordant with expectations in key ways. For example, the primate CGE might be expected to  
516 harbor evolutionary novelties in its interneuron repertoire because it generates a larger proportion  
517 of interneurons in primates than in rodents<sup>49</sup>, because CGE interneurons are born later than MGE  
518 interneurons, and because CGE interneurons preferentially occupy the expanded upper  
519 neocortical layers<sup>50</sup>. However, the most striking cellular aspects of rodent–primate divergence in  
520 the cortex, hippocampus, and striatum involved interneurons whose RNA expression patterns  
521 indicated that they originated in the MGE. Similarly, although the neocortex has attracted intense  
522 interest because it is a highly evolved and specialized structure that is thought to underlie  
523 expansions in primate cognitive capability, it was in the striatum that we identified a primate  
524 interneuron type with no mouse homolog. The systematic analysis of many more species and cell  
525 types may reveal more such examples of evolutionary flexibility and innovation.

526  
527

## REFERENCES

- 528 1. Northcutt, R. G. & Kaas, J. H. The emergence and evolution of mammalian  
529 neocortex. *Trends in Neurosciences* **18**, 373–379 (1995).
- 530 2. Laclef, C. & Métin, C. Conserved rules in embryonic development of cortical  
531 interneurons. *Seminars in Cell and Developmental Biology* **76**, 86–100 (2018).
- 532 3. Barkan, C. L., Kelley, D. B. & Zornik, E. Premotor neuron divergence reflects vocal  
533 evolution. *J. Neurosci.* **38**, 5325–5337 (2018).
- 534 4. Peng, Y.-R. *et al.* Molecular Classification and Comparative Taxonomics of Foveal  
535 and Peripheral Cells in Primate Retina. *Cell* **176**, 1222–1237.e22 (2019).
- 536 5. Katz, P. S. & Harris-Warrick, R. M. The evolution of neuronal circuits underlying  
537 species-specific behavior. *Current Opinion in Neurobiology* **9**, 628–633 (1999).
- 538 6. Tosches, M. A. *et al.* Evolution of pallium, hippocampus, and cortical cell types  
539 revealed by single-cell transcriptomics in reptiles. *Science* **360**, 881–888 (2018).
- 540 7. Hodge, R. D. *et al.* Conserved cell types with divergent features between human  
541 and mouse cortex. *bioRxiv.org*  
542 (2018). doi:10.1101/384826
- 543 8. Xu, X. *et al.* Species and cell-type properties of classically defined human and  
544 rodent neurons and glia. *eLIFE* **7**, 1–47 (2018).
- 545 9. Kepecs, A. & Fishell, G. Interneuron cell types are fit to function. *Nature* **505**, 318–  
546 326 (2014).
- 547 10. Tosches, M. A. & Laurent, G. Evolution of neuronal identity in the cerebral cortex.  
548 *Current Opinion in Neurobiology* **56**, 199–208 (2019).

- 549 11. Tasic, B. *et al.* Shared and distinct transcriptomic cell types across neocortical  
550 areas. 1–37 (2017). doi:10.1101/229542
- 551 12. Saunders, A. *et al.* Molecular Diversity and Specializations among the Cells of the  
552 Adult Mouse Brain. *Cell* **174**, 1015–1030 (2018).
- 553 13. Macosko, E. Z. *et al.* Highly Parallel Genome-wide Expression Profiling of Individual  
554 Cells Using Nanoliter Droplets. *Cell* **161**, 1202–1214 (2015).
- 555 14. Paul, A. *et al.* Transcriptional Architecture of Synaptic Communication Delineates  
556 GABAergic Neuron Identity. *Cell* **171**, 522–525.e20 (2017).
- 557 15.erculano-Houzel, S. The remarkable, yet not extraordinary, human brain as a  
558 scaled-up primate brain and its associated cost. *Proc Natl Acad Sci USA* **109**,  
559 10661–10668 (2012).
- 560 16. Kim, Y. *et al.* Brain-wide Maps Reveal Stereotyped Cell-Type- Based Cortical  
561 Architecture and Subcortical Sexual Dimorphism. *Cell* **171**, 456–460.e22 (2017).
- 562 17. Florio, M., Borrell, V. & Huttner, W. B. Human-specific genomic signatures of  
563 neocortical expansion. *Current Opinion in Neurobiology* **42**, 33–44 (2017).
- 564 18. Lui, J. H., Hansen, D. V. & Kriegstein, A. R. Development and Evolution of the  
565 Human Neocortex. *Cell* **146**, 18–36 (2011).
- 566 19. Brito, R. B. & (null), G. F. The developmental integration of cortical interneurons into  
567 a functional network. *Current Topics in Developmental Biology* **87**, 81–118 (2009).
- 568 20. Ataman, B. *et al.* Evolution of Osteocrin as an activity- regulated factor in the  
569 primate brain. *Nature* **539**, 242–247 (2016).
- 570 21. Lek, M. *et al.* Analysis of protein-coding genetic variation in 60,706 humans. *Nature*  
571 **536**, 285–291 (2016).
- 572 22. Welch, J., Kozareva, V., Ferreira, A., bioRxiv, C. V.2018. Integrative inference of  
573 brain cell similarities and differences from single-cell genomics. *biorxiv.org*  
574 doi:10.1101/459891
- 575 23. Tasic, B. *et al.* Shared and distinct transcriptomic cell types across neocortical  
576 areas. *Nature* **563**, 1–41 (2018).
- 577 24. Wester, J. C. *et al.* Neocortical Projection Neurons Instruct Inhibitory Interneuron  
578 Circuit Development in a Lineage- Dependent Manner. *Neuron* **102**, 960–975.e6  
579 (2019).
- 580 25. Lodato, S. *et al.* Excitatory Projection Neuron Subtypes Control the Distribution of  
581 Local Inhibitory Interneurons in the Cerebral Cortex. *Neuron* **69**, 763–779 (2011).
- 582 26. Sur, M. & Rubenstein, J. L. R. Patterning and plasticity of the cerebral cortex.  
583 *Science* **310**, 805–810 (2005).
- 584 27. Miller, J. A. *et al.* Transcriptional landscape of the prenatal human brain. *Nature*  
585 **508**, 199–206 (2014).
- 586 28. Hawrylycz, M. J. *et al.* An anatomically comprehensive atlas of the adult human  
587 brain transcriptome. *Nature* **489**, 391–399 (2012).
- 588 29. Nowakowski, T. J. *et al.* Spatiotemporal gene expression trajectories reveal  
589 developmental hierarchies of the human cortex. *Science* **358**, 1318–1323 (2017).
- 590 30. Margulies, D. S. *et al.* Situating the default-mode network along a principal gradient  
591 of macroscale cortical organization. *Proc Natl Acad Sci USA* **113**, 12574–12579  
592 (2016).
- 593 31. Krienen, F. M., Yeo, B. T. T., Ge, T., Buckner, R. L. & Sherwood, C. C.  
594 Transcriptional profiles of supragranular-enriched genes associate with  
595 corticocortical network architecture in the human brain. *Proc Natl Acad Sci USA*  
596 **113**, E469–E478 (2016).
- 597 32. Tasic, B. *et al.* Adult mouse cortical cell taxonomy revealed by single cell  
598 transcriptomics. *Nat. Neurosci.* **19**, 335–346 (2016).

- 599 33. Tosches, M. A. Developmental and genetic mechanisms of neural circuit evolution.  
600 *Developmental Biology* **431**, 16–25 (2017).
- 601 34. Mayer, C. *et al.* Developmental diversification of cortical inhibitory interneurons.  
602 *Nature* **555**, 457–462 (2018).
- 603 35. Tricoire, L. *et al.* Common Origins of Hippocampal Ivy and Nitric Oxide Synthase  
604 Expressing Neurogliaform Cells. *Journal of Neuroscience* **30**, 2165–2176 (2010).
- 605 36. Nóbrega-Pereira, S. *et al.* Postmitotic Nkx2-1 Controls the Migration of  
606 Telencephalic Interneurons by Direct Repression of Guidance Receptors. *Neuron*  
607 **59**, 733–745 (2008).
- 608 37. Jakovcevski, I., Mayer, N. & Zecevic, N. Multiple Origins of Human Neocortical  
609 Interneurons Are Supported by Distinct Expression of Transcription Factors.  
610 *Cerebral Cortex* **21**, 1771–1782 (2010).
- 611 38. Tricoire, L. *et al.* A Blueprint for the Spatiotemporal Origins of Mouse Hippocampal  
612 Interneuron Diversity. *Journal of Neuroscience* **31**, 10948–10970 (2011).
- 613 39. Boldog, E. *et al.* Transcriptomic and morphophysiological evidence for a specialized  
614 human cortical GABAergic cell type. *Nat. Neurosci.* **21**, 1185–1195 (2018).
- 615 40. Buckner, R. L. & Krienen, F. M. The evolution of distributed association networks in  
616 the human brain. *Trends Cogn. Sci.* **17**, 648–665 (2013).
- 617 41. Florio, M. *et al.* Human-specific gene ARHGAP11B promotes basal progenitor  
618 amplification and neocortex expansion. *Science* **347**, 1465–1470 (2015).
- 619 42. Muñoz Manchado, A. B. *et al.* Diversity of Interneurons in the Dorsal Striatum  
620 Revealed by Single-Cell RNA Sequencing and PatchSeq. *Cell Reports* **24**, 2179–  
621 2190.e7 (2018).
- 622 43. Graveland, G. A. & Difiglia, M. The frequency and distribution of medium-sized  
623 neurons with indented nuclei in the primate and rodent neostriatum. *Brain Res.* **327**,  
624 307–311 (1985).
- 625 44. Arendt, D. *et al.* The origin and evolution of cell types. *Nat Rev Genet* **17**, 744–757  
626 (2016).
- 627 45. Zeng, H. & Sanes, J. R. Neuronal cell-type classification: challenges, opportunities  
628 and the path forward. *Nat Rev Neurosci* **18**, 530–546 (2017).
- 629 46. Huang, Z. J. & Paul, A. The diversity of GABAergic neurons and neural  
630 communication elements. *Nat Rev Neurosci* 1–10 (2019). doi:10.1038/s41583-019-  
631 0195-4
- 632 47. Middleton, F. A. & Strick, P. L. Basal Ganglia Output and Cognition: Evidence from  
633 Anatomical, Behavioral, and Clinical Studies. *Brain and Cognition* **42**, 183–200  
634 (2000).
- 635 48. Oláh, S. *et al.* Regulation of cortical microcircuits by unitary GABA-mediated  
636 volume transmission. *Nature* **461**, 1278–1281 (2009).
- 637 49. Hladnik, A., Džaja, D., Darmopil, S., Jovanov-Milošević, N. & Petanjek, Z. Spatio-  
638 temporal extension in site of origin for cortical calretinin neurons in primates. *Front*  
639 *Neuroanat* **8**, 50 (2014).
- 640 50. Miyoshi, G. *et al.* Genetic Fate Mapping Reveals That the Caudal Ganglionic  
641 Eminence Produces a Large and Diverse Population of Superficial Cortical  
642 Interneurons. *Journal of Neuroscience* **30**, 1582–1594 (2010).
- 643

644

645 **Acknowledgments**

646 This work was supported by the Broad Institute's Stanley Center for Psychiatric Research and  
647 Brain Initiative grant U01MH114819 to G. Feng and S.A.M, by the Dean's Innovation Award  
648 (Harvard Medical School) to G. Fishell and S.A.M., and by the Hock E. Tan and K. Lisa Yang  
649 Center for Autism Research at MIT, the Poitras Center for Psychiatric Disorders Research at  
650 MIT and the McGovern Institute for Brain Research at MIT (G. Feng). Also supported by NINDS  
651 RO1NS032457 (C.A.W.). C.A.W. is an Investigator of the Howard Hughes Medical Institute. We  
652 thank Dr. Maude W. Baldwin, Avery D. Bell, Steven Burger, Dr. Christopher Patil, and Dr. Randy  
653 L. Buckner for comments on manuscript drafts; Dr. Christian Mayer for analysis advice; and Dr.  
654 Christina Usher for assistance with manuscript preparation.

655

656 **Author Contributions**

657 F.M.K, S.A.M., G. Feng, and G. Fishell designed the study. F.M.K. prepared and dissected tissue;  
658 L.B. and M.G. developed the nuclei Drop-seq protocol. M.G., A.L., C.D.M., N.R., E.B., and L.B.  
659 performed Drop-seq and prepared sequencing libraries. M.G. performed sequencing, alignment,  
660 and QC analysis. F.M.K., A.S., J.N., A.W., D.K. R.d.R., and S.A.M. developed analysis pipelines.  
661 F.M.K. analyzed the data with input from S.A.M, G. Fishell, M.F., A.L. and A.S. D.K. developed the  
662 web resource. Q.Z., C.W., M.B., V.T., R.S., C.A.W., L.K., S.B., and G. Feng provided tissue for Drop-  
663 seq and smFISH experiments. K.L., H.Z., C.D.K., N.R., E.B., M.F-O., J.L., F.M.K. and J.D. performed  
664 and analyzed smFISH experiments. R.M., B.S., and B.R. contributed fate-mapping experiments.  
665 F.M.K and S.A.M wrote the paper with input from coauthors.

666

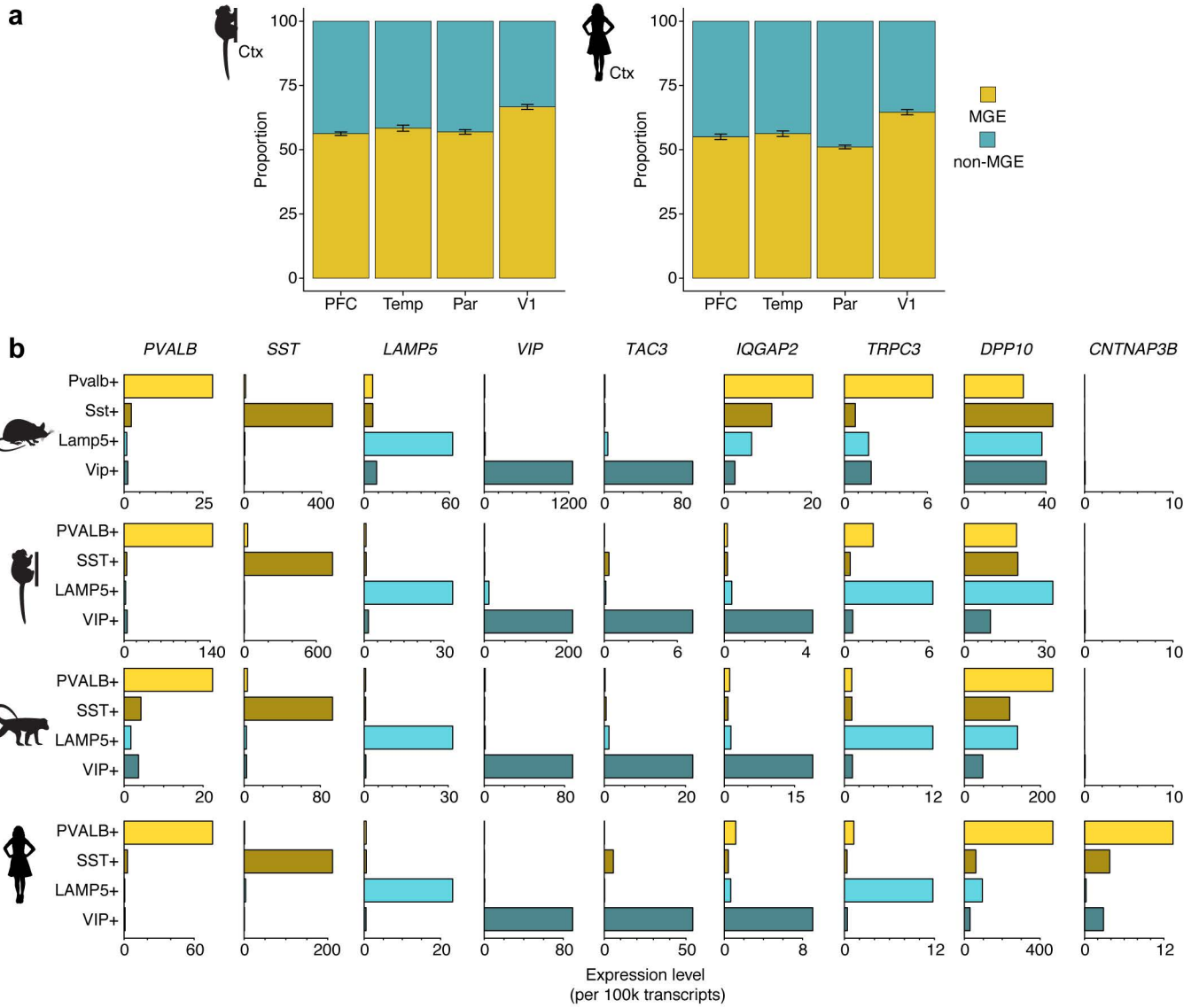
667 **Extended Data Table 1.** Specimen information table.

668 **Extended Data Table 2.** Reagent and resource table.

669

670

# Extended Data Figure 1



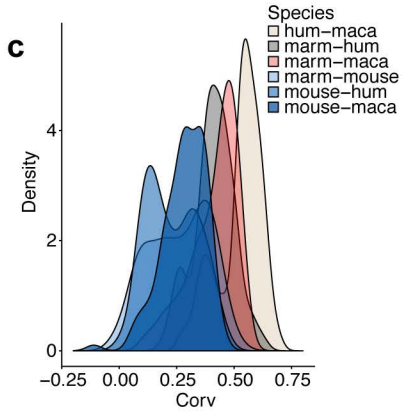
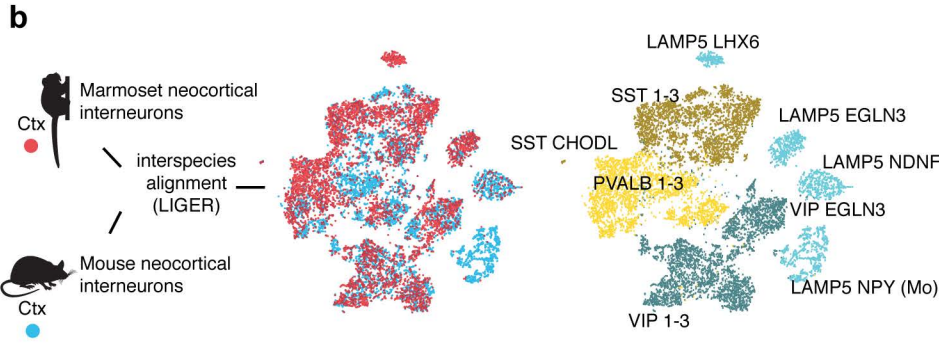
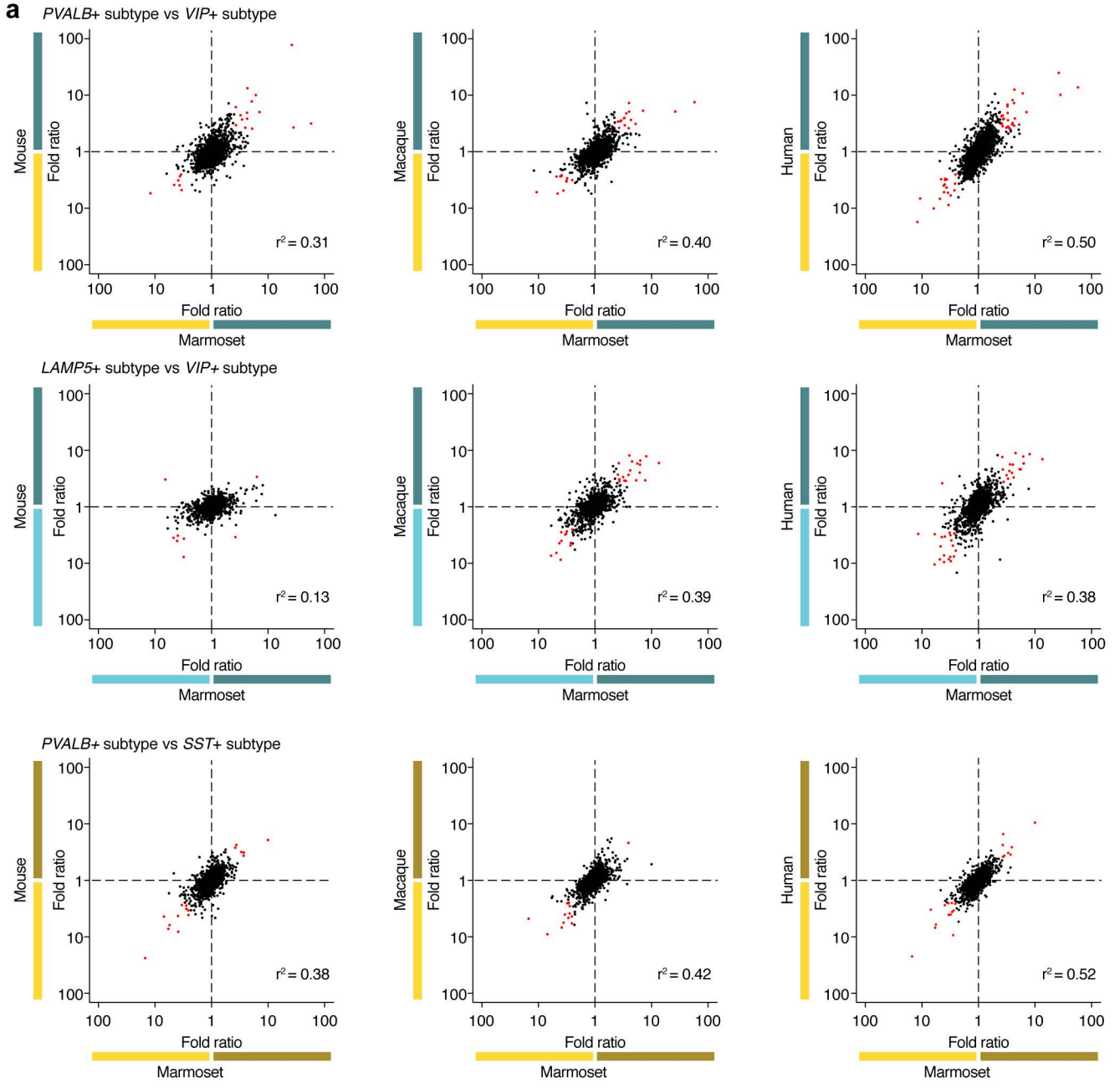
671 **Extended Data Figure 1. Interneuron abundances and gene expression in neocortex.**

672 **a**, Proportion of MGE and non-MGE interneurons in cortical association areas (prefrontal cortex,  
673 temporal pole, and lateral parietal association cortex) and in primary visual area (V1) in marmoset  
674 and human. Error bars represent binomial confidence intervals. **b**, Examples of markers that are  
675 consistent, or that vary across species, within the four primary interneuron classes. Values are  
676 scaled counts per 100k transcripts.

677

678

# Extended Data Figure 2



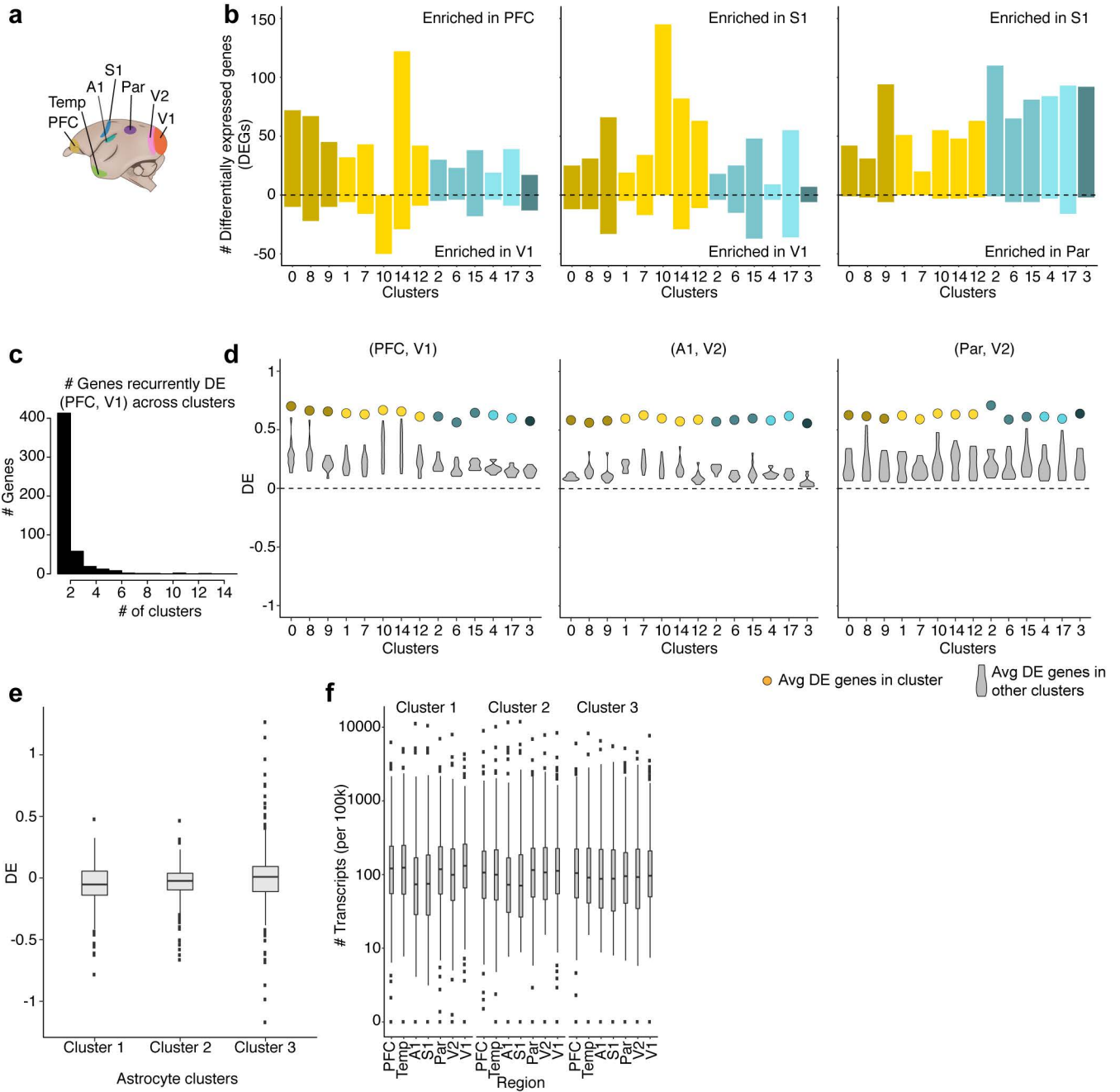


679 **Extended Data Figure 2. Pairwise comparisons of neocortical interneuron types across**  
680 **species. a**, Fold difference of each expressed gene between types of MGE-derived interneurons  
681 and types of CGE-derived interneuron across pairs of species. Genes in red have >3-fold  
682 expression difference in either cell type in each species pair. **b**, (left) LIGER integration of  
683 marmoset (red dots) and mouse (teal dots) neocortical interneurons. (right) Same t-SNE with  
684 clusters colored by interneuron class (colors as in Fig. 1). **c**, Density histogram of correlation ( $r$ )  
685 values of fold differences computed for each possible cluster pair from LIGER species-integrated  
686 analyses. Each density trace corresponds to a species pair; blue traces indicate primate–mouse  
687 comparisons, and other colors indicate primate–primate comparisons.

688

689

# Extended Data Figure 3



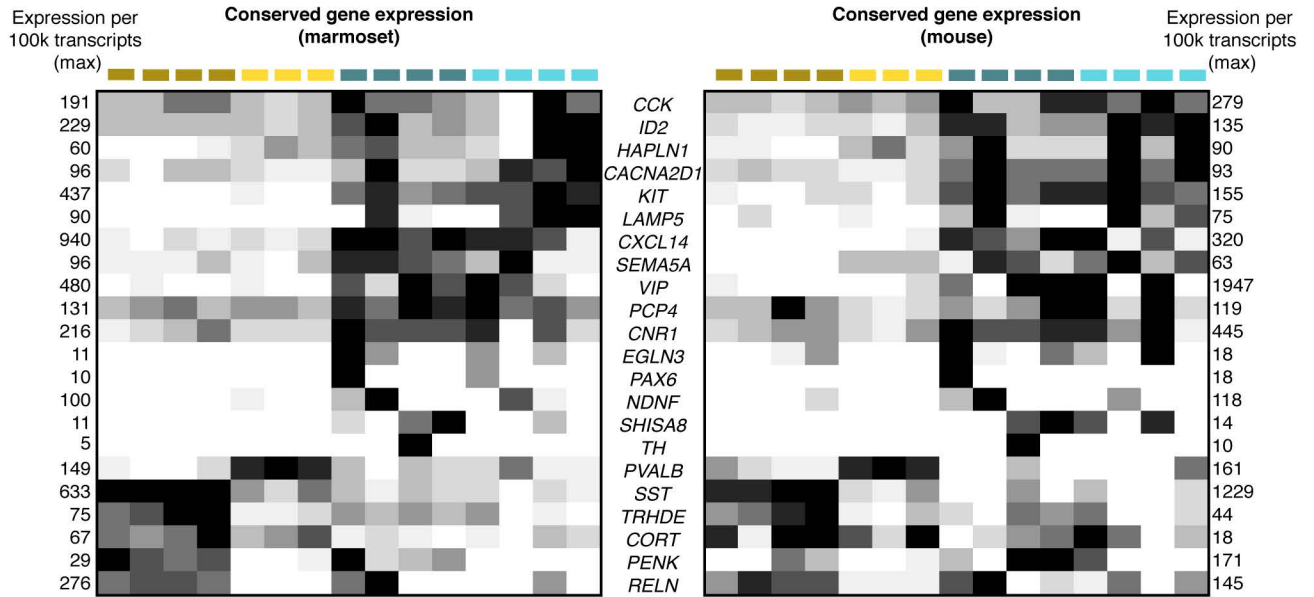
690 **Extended Data Figure 3. Regional gene expression variation in neocortex. a**, Schematic of  
691 neocortical region locations in marmoset. **b**, Histogram of the number of regionally differentially  
692 expressed genes (rDEGs) (>3-fold expression difference) between three representative pairs of  
693 regions, in each cell type (cluster) for which there were at least 50 cells per region. **c**, Histogram  
694 of the number of interneuron clusters (cell types) in which a given gene is differentially expressed.  
695 At a threshold of >3-fold, most genes are only differentially expressed in a single cell type (cluster).  
696 **d**, Colored dots represent average fold difference of DEGs in each cluster in marmoset  
697 interneurons. Violin plots represent the distribution of average fold differences in each cluster (cell  
698 type) when using rDEGs from other clusters. Three representative region pairs are shown. **d**, Fold  
699 ratios ( $\log_{10}$ ) between PFC and V1 for three astrocyte subtypes ( $n = 32,600$  nuclei) in marmosets  
700 using rDEGs identified between PFC and V1 in interneurons. **e**, Expression in astrocytes of genes  
701 that exhibited an anterior–posterior expression gradient in interneurons. Regions are arranged in  
702 anterior–posterior order on the x axis.

703

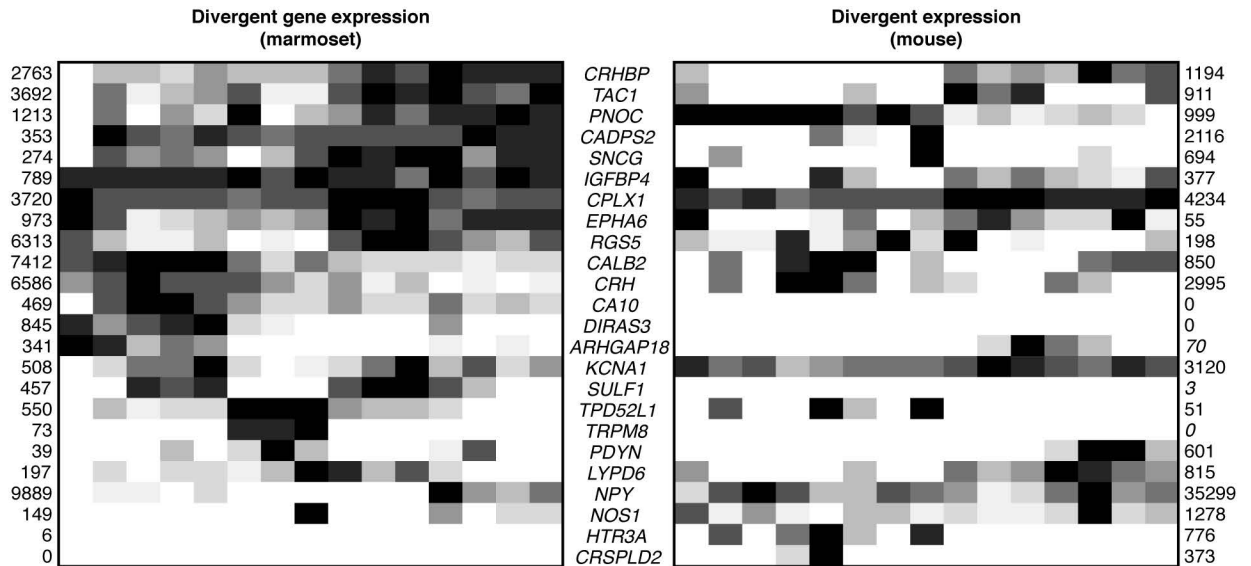
704

# Extended Data Figure 4

**a**

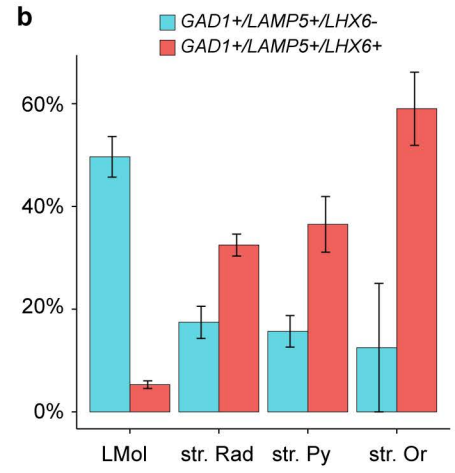
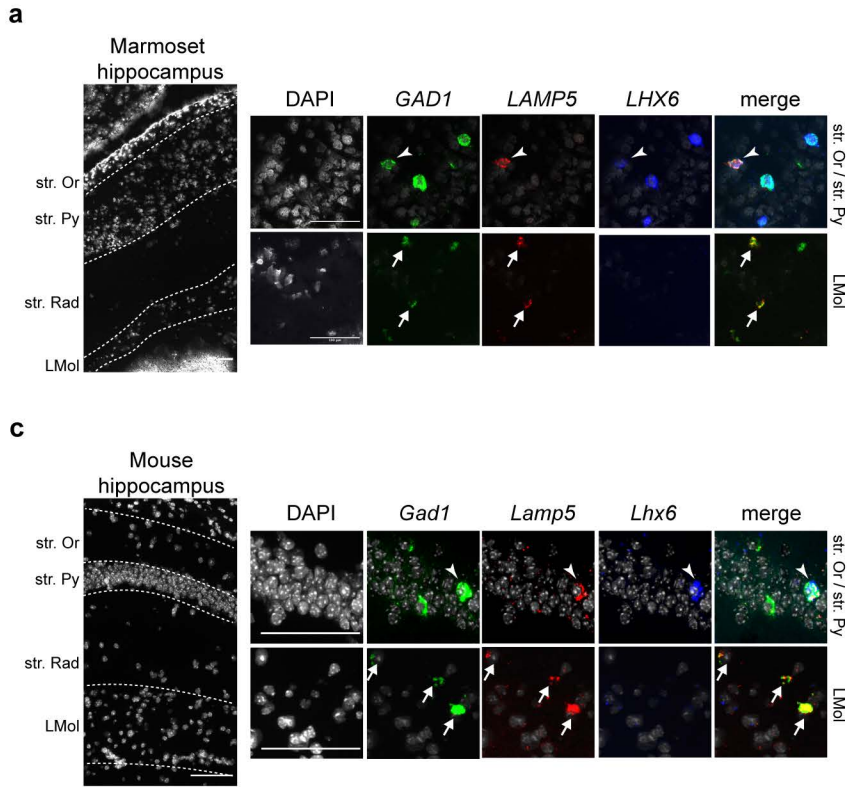


**b**



705 **Extended Data Figure 4. Conserved and divergent gene expression across neocortical**  
706 **types. a,** Heat map of exemplar genes that had consistent patterns of expression in LIGER  
707 integrated marmoset–mouse clusters from Extended Data Fig. 2b. Each gene (row) is scaled to  
708 the scaled max (black) expression (values given outside plots) for each species separately. **b,**  
709 Heatmap of exemplar genes that have divergent expression patterns in LIGER-integrated  
710 marmoset–mouse clusters from Extended Data Fig. 2b. Each gene (row) is scaled to the scaled  
711 max (black) expression (values given outside plots) for each species separately.  
712  
713

# Extended Data Figure 5

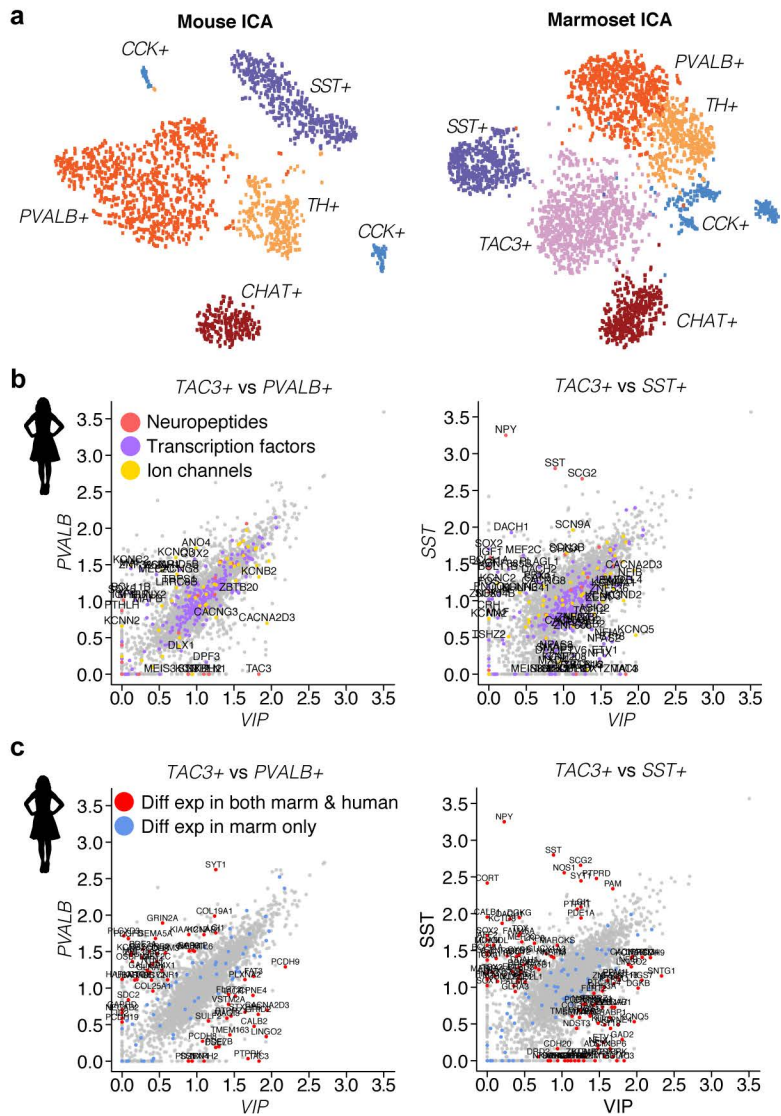


714 **Extended Data Figure 5. LAMP5+ interneuron types in hippocampus.** **a**, Single-molecule  
715 fluorescence in situ hybridization (smFISH) for *GAD1*, *LAMP5*, and *LHX6* in marmoset  
716 hippocampal layers (CA1/CA2 subfields). Arrowhead indicates triple positive cells; arrow  
717 indicates the *LHX6*- population. (*top row*) Strata oriens (Str. Or) and strata pyramidale (Str. Py).  
718 (*bottom row*) strata lacunosum moleculare (LMol). Scale bars = 100  $\mu$ m. **b**, Quantification of  
719 *GAD1/LAMP5/LHX6*+ (green) and *GAD1/LAMP5/LHX6*- cells as percentage of all *GAD1*+ cells  
720 in marmoset hippocampus (compare to mouse data in<sup>38</sup>). **c**, smFISH for *Gad1*, *Lamp5*, and *Lhx6*  
721 in mouse hippocampal layers (CA1).

722

723

Extended Data Figure 6





724 **Extended Data Figure 6. Interneuron types in striatum. a**, t-SNE representations of ICA-based  
725 clustering for mouse and marmoset striatal interneurons. **b**, Gene expression differences in  
726 human caudate between *TAC3+* and *PVALB+* (left) or *TAC3+* and *SST+* (right) populations.  
727 Neuropeptides (red) and transcription factors (blue) are labeled. **c**, Same data as in **b**, but instead  
728 highlighting genes that were differentially expressed in both marmoset and human (red), or only  
729 in marmoset (blue).  
730

731 **METHODS**

732

733 Specimen information is available in Extended Data Table 1.

734 Reagent information is available in Extended Data Table 2.

735

736 **Specimens and Donors for Nuclei Drop-seq**

737

738 *Mouse.* Mouse experiments were approved by and in accordance with Harvard Medical School  
739 IACUC protocol number IS00000055-3. Sections of frontal and visual cortex were prepared from  
740 male and female adult mice (60–70 days old; C57Blk6/N, Charles River Labs Stock #027). Mice  
741 were deeply sedated with isoflurane and transcardially perfused with ice-cold Sucrose-HEPES  
742 buffer described in<sup>1</sup>, which contains (in mM) 110 NaCl, 2.5 KCl, 10 HEPES, 7.5 MgCl<sub>2</sub>, 25 glucose,  
743 75 sucrose (~350 mOsm/kg<sup>-1</sup>); sectioned; and flash-frozen on liquid nitrogen.

744

745 *Marmoset.* Marmoset experiments were approved by and in accordance with Massachusetts  
746 Institute of Technology IACUC protocol number 051705020. Three adult marmosets (1.5–2 years  
747 old; one male, 2 females) were deeply sedated by intramuscular injection of ketamine (20-40  
748 mg/kg) or alfaxalone (5-10 mg/kg), followed by intravenous injection of sodium pentobarbital (10–  
749 30 mg/kg). When pedal withdrawal reflex was eliminated and/or respiratory rate was diminished,  
750 animals were transcardially perfused with ice-cold Sucrose-HEPES buffer. Whole brains were  
751 rapidly extracted into fresh buffer on ice. Sixteen 2-mm coronal blocking cuts were rapidly made  
752 using a custom-designed marmoset brain matrix. Slabs were transferred to a dish with ice-cold  
753 Dissection Buffer<sup>1</sup>, and regions of interest were dissected using a marmoset atlas as reference<sup>2</sup>.  
754 Regions were snap-frozen in liquid nitrogen and stored in individual microcentrifuge tubes at -  
755 80°C.

756

757 *Macaque*. Whole brains from two healthy, immunologically and treatment-naive adult macaques  
758 (2 males; 10–11 years old) were obtained from terminal experiments (IACUC 4315-02). Animals  
759 were deeply sedated with ketamine and euthanized by pentobarbital overdose, and transcardially  
760 perfused with ice-cold Sucrose-HEPES buffer. Brains were rapidly blocked in ~5-mm coronal  
761 slabs and frozen in liquid nitrogen or isopentane on dry ice.

762

763 *Human*. Frozen tissue was obtained from the Harvard Brain Tissue Resource Center (HBTRC;  
764 McLean Hospital). Four donors were used for analysis of striatal interneurons, and two for  
765 analysis of neocortical interneurons. History of psychiatric or neurological disorders was ruled out  
766 by consensus diagnosis carried out by retrospective review of medical records and extensive  
767 questionnaires concerning social and medical history provided by family members. Several  
768 regions from each brain were examined by a neuropathologist. The cohort used for this study did  
769 not include subjects with evidence of gross and/or macroscopic brain changes, or clinical history,  
770 consistent with cerebrovascular accident or other neurological disorders. Subjects with Braak  
771 stages III or higher (modified Bielschowsky stain) were not included. None of the subjects had  
772 significant history of substance dependence within 10 or more years of death, as further  
773 corroborated by negative toxicology reports.

774

#### 775 **Nuclei Drop-seq library preparation and sequencing**

776 Nuclei suspensions were prepared from frozen tissue and used for Nuclei Drop-seq following the  
777 protocol described at <https://protocols.io/view/extraction-of-nuclei-from-brain-tissue-2srged6>.  
778 Drop-seq libraries were prepared as previously described<sup>3</sup> with modifications, quantification, and  
779 QC as described in<sup>1</sup>, as well as the following modifications optimized for nuclei: in the Drop-seq  
780 lysis buffer, 8 M guanidine hydrochloride (pH 8.5) was substituted for water, nuclei were loaded  
781 into the syringe at a concentration of 176 nuclei/ $\mu$ L, and cDNA amplification was performed using  
782 around 6000 beads per reaction (15 PCR cycles were used for marmoset nuclei, and 16 for

783 macaque and human nuclei). Raw sequencing reads were aligned to the following genome  
784 assemblies: GRCm38.81 (mouse), calJac3 (marmoset), Mmul8.0.1 (macaque), and hg19  
785 (human). Reads that mapped to exons or introns of each assembly were assigned to annotated  
786 genes.

787

### 788 **Mouse single-cell dataset**

789 Interneurons were curated *in silico* from the single-cell datasets available in <sup>1</sup> from available  
790 structures: frontal and posterior neocortex, striatum, cerebellum, thalamus, hippocampus,  
791 substantia nigra, and entopeduncular nucleus.

792

### 793 **Single species independent component analysis (ICA)**

794 Initial analyses to identify interneurons based on marker expression were conducted on each  
795 species separately. Nuclei with fewer than 300 detected genes were removed from analysis.  
796 Briefly, independent component analysis (ICA, using the fastICA package in R) was performed  
797 on each species and each region's digital gene expression (DGE) matrix separately after  
798 normalization and variable gene selection as in <sup>1</sup>. These first-round individual-species analyses  
799 produced clustering solutions with ~8–11 clusters of major cell types (neurons, glia, vasculature),  
800 from which interneuron clusters could be identified based on canonical markers (e.g. *GAD1*,  
801 *GAD2*). The raw DGEs were subsetted to include only cells from these clusters to form new,  
802 interneuron-only DGEs. Normalization, variable gene selection, and ICA was repeated on these  
803 interneuron-only DGEs, but this time the full ICA curation pipeline described in <sup>1</sup> was used to  
804 identify doublets, outliers, artifactual signals, and biological components of interest. Cells  
805 identified by this procedure as doublets or outliers were removed from the DGEs, and these  
806 filtered DGEs were then carried forward for integrated analyses across regions and/or species  
807 using LIGER<sup>4</sup>.

808

809 **Interneuron abundances and local specialization in neocortex**

810 Proportions of *PVALB*+ or *SST*+ (MGE-derived) and *VIP*+ or *LAMP5*+ (non-MGE derived) were  
811 calculated for each species separately for frontal association areas (FC, mouse) or prefrontal  
812 cortex (PFC, primates) and visual cortex (V1). Cells were allocated to MGE or non-MGE pools  
813 based on their cluster assignment in individual-species ICA clustering. Error bars represent 95%  
814 confidence intervals for binomial probability, computed with the R package Hmisc.

815  
816  
817

818 **Identification of conserved and divergent genetic programs within conserved interneuron**

819 **types**

820 Interneurons from the neocortex of each species were partitioned into four main classes based  
821 on marker expression (*VIP*, *LAMP5*, *PVALB*, *SST*). (We also detected a rare and distinct, fifth  
822 category of cortical GABAergic cell – *MEIS2*+ cells – which in mouse reside in deep layer white  
823 matter and make long-range projections. However, consistent with other reports<sup>5</sup>, this type was  
824 inconsistently observed across individual animals and regions, likely due to its laminar location  
825 and low abundance, and was not analyzed further.)

826

827 For each species and each of the four main classes, transcripts were pooled across cells,  
828 normalized by total number of transcripts, and scaled to 100k transcripts, which yielded four  
829 vectors of representative gene expression for each class. We then applied a series of filters to  
830 search all expressed genes for those that were selectively expressed by at least one of the four  
831 cell types in at least one species. Genes with low expression (<10 transcripts per 100k in any  
832 species) were removed. At least one species had to show a >3-fold difference between the  
833 maximum and minimum expression level across the four types. These filters identified an initial  
834 set of putative markers in one or more species. To search for genes that were consistent or  
835 differed across species, for each gene (only one-to-one orthologues were considered), Pearson

836 correlations between pairs of species were computed, yielding six correlation values. If a gene  
837 was not detected in a given species, values were set to 0 for pairs that included that species.

838

### 839 **Quantitative expression level comparisons across neocortical classes**

840 To examine the extent to which evolution has constrained a gene's quantitative expression level  
841 across the four main neocortical cell classes, we focused on meaningfully expressed genes (4051  
842 genes that exhibited at least 1.5-fold expression variation across the four classes in at least one  
843 species, and were also present with an abundance of at least 10 transcripts per 100k in at least  
844 one cell class). This gene list was intersected with a set of genes predicted to be intolerant of loss  
845 of function (pLI > 0.9) across 60,706 humans<sup>6</sup>, yielding a set of 1286 genes that were meaningfully  
846 expressed in interneurons and showed evidence of intolerance to protein-truncating variants.  
847 Pearson correlations were computed on the vector of expression values for each of these genes  
848 in all possible pairs of species.

849

### 850 **Species comparisons of differential expression amongst pairs of cell types**

851 Integrated species analyses were performed using LIGER<sup>4</sup> between species pairs, which had the  
852 advantage of allowing each pair of species to jointly determine cluster definition. Parameter values  
853 were explored over a range using LIGER functions to suggest optimal values; the resultant  
854 clusterings (e.g. Extended Data Fig. 2) used the following parameters: variance threshold = 0.15  
855 (for inclusion of genes into LIGER alignment),  $k = 25$  (number of factors),  $\lambda = 5$   
856 (regularization parameter to penalize dataset-specific influence on alignment), resolution = 0.8  
857 (controls resolution of clusters in community detection). For each cluster, the expression values  
858 of meaningfully expressed genes (at least 10 transcripts per 100k in both species) were extracted  
859 and fold differences for each gene was computed relative to each other cluster for each of the  
860 species independently. These fold differences were then correlated across pairs of species.

861

862

### 863 **Neocortical regionally differentially expressed genes (rDEGs)**

864

865 To examine gene expression variation across neocortical regions in marmoset, region (n=7)

866 datasets were pooled into a region-integrated LIGER analysis (variance threshold = 0.15, k = 25,

867  $\lambda = 5$ , resolution = 0.8). These parameters produced 17 clusters; two clusters were removed

868 for having fewer than 50 cells from one or more regions, yielding in a final set of 15 clusters for

869 cross-region comparisons. For each cluster, differential expression was computed between all

870 region pairs using a fold-difference threshold of 3.

871

#### 872 *Interneuron rDEGs in astrocytes*

873 Marmoset neocortical astrocytes were analyzed by identifying the cluster(s) that expressed known

874 astrocyte markers (e.g. *AQP4*, *GFAP*, *GJA1*, *GLUL*) from the same individuals used in

875 interneuron analyses. Cells in these clusters were isolated from raw data and clustered using the

876 ICA pipeline described above, which resulted in three astrocyte subtypes. For each astrocyte

877 subcluster, fold differences of rDEGs identified in interneurons (in comparisons of PFC to V1)

878 were computed for PFC and V1 in astrocytes.

879

#### 880 *Marmoset interneuron rDEGs profiled in macaque, human and mouse*

881 Marmoset interneuron rDEGs (identified in comparisons of PFC to V1) were profiled in other

882 species: for each rDEG, fold differences between frontal/prefrontal cortex and V1 cells were

883 computed for each cluster identified by each species' ICA-based clustering. The percentage and

884 median differential expression ( $\log_{10}$ -transformed fold differences) of genes that were rDEGs in

885 marmoset and were also rDEG was calculated in each species.

886

#### 887 *Spatial correlations*

888 For each cluster, expression levels of rDEGs identified in comparisons between PFC and V1 were  
889 examined in the other neocortical regions (n = 5). To quantify the existence of spatial gradients,  
890 for each gene the Pearson correlation between expression and spatial order along the anterior–  
891 posterior axis was computed in the five remaining regions in order (Temp, S1, A1, Par, V2). Mean  
892 correlation values were compared to a null distribution obtained by permuting the ordering (120  
893 possible orderings).

894

### 895 **Hierarchical clustering**

896 Dendrograms of cell-type relationships were produced using hierarchical clustering (using the  
897 hclust function, method = complete, in R) of genes normalized (to 100k transcripts), using log<sub>10</sub>  
898 transformed values of all expressed genes (genes with at least 10 transcripts per 100k  
899 transcripts).

900

901

### 902 **Single-molecule fluorescent *in situ* hybridization (smFISH)**

903

#### 904 *Neocortex and hippocampus*

905 Frozen, unfixed tissue sections (12 μm) of mouse (P60-P70; Charles River, C57BL/6; n = 2),  
906 marmoset (n = 2), and ferret (n = 1) brain tissue were cut on a cryostat (Leica CM 1950), adhered  
907 to SuperFrost Plus microscope slides (Fisher Scientific, 12-550-15) and processed for three-color  
908 smFISH using the ACD v2 RNAscope multiplexed fluorescence protocol for fresh frozen tissue.  
909 Probes are listed in Extended Data Table 2. The ferret (*Mustela putorius furo*) was sourced from  
910 Marshall Bioresources, and was used according to protocols approved by IACUC of Boston  
911 Children's Hospital.

912

#### 913 *In situ–based quantification of neocortical & hippocampal LAMP5+ subtypes*



914 For hippocampus and neocortical area S1, laminar boundaries were identified with DAPI stains  
915 in mouse and marmoset tissue. Neocortical laminae were separated into five bins (layer 1, layer  
916 2/3, layer 4, layer 5, layer 6); hippocampal laminae within CA1 and CA2 regions were separated  
917 into four bins. Within each bin, *GAD1+*, *GAD1+/LAMP5+*, and *GAD1+/LAMP5+/LHX6+* cells were  
918 counted in two sections of each replicate. In total, 3998 cells were counted.

919

#### 920 *Single-molecule FISH (smFISH) in marmoset striatum*

921 One male marmoset (age = 6 years) was euthanized and perfused with ice-cold saline. The whole  
922 brain was immediately removed, embedded in Optimal Cutting Temperature (OCT) freezing  
923 medium, and flash-frozen in an isopropyl ethanol-dry ice bath. Samples were cut into 16  $\mu\text{m}$   
924 sections on a cryostat (Leica CM 1850), adhered to SuperFrost Plus microscope slides (Fisher  
925 Scientific, 12-550-15), and stored at  $-80^{\circ}\text{C}$  until use. Samples were immediately fixed in 4%  
926 paraformaldehyde and stained on the slide according to the Advanced Cell Diagnostics  
927 RNAscope Multiplex Fluorescent Reagent Kit v2 Assay (ACD, 323100) protocol. Samples were  
928 stained for *VIP* (ACD, 554571-C2) and *NKX2-1* (ACD, 532751-C3) with antisense probes, and  
929 coverslipped with Vectashield HardSet Antifade mounting medium with DAPI (Vector  
930 Laboratories, H-1500). Z-stack serial images were taken through the whole depth on a Nikon Ti  
931 Eclipse inverted microscope with an Andor CSU-W1 confocal spinning disc unit and an Andor  
932 DU-888 EMCCD using a 20 $\times$ , 0.75 NA air objective, and later max-projected in FIJI (ImageJ,  
933 NIH). Fields of view were randomly chosen across the whole striatal sample. Probes listed in  
934 Extended Data Table 2.

935

#### 936 **Fate mapping of *Lamp5+/Lhx6+* cells in mouse hippocampus and neocortex**

937 To label *Lamp5+/Lhx6+* cells in the mouse neocortex and hippocampus, we utilized an  
938 intersectional genetics approach. In mouse mature cortical interneurons, *Id2* and *Lamp5* are  
939 expressed in nearly identical populations<sup>7</sup>, and so we utilized an *Id2-CreER* driver line<sup>8</sup> (Jax

940 stock# 016222) in combination with an Nkx2.1-Flpo driver<sup>9</sup> (Jax stock# 028577) and the Cre/Flp  
941 dependent tdTomato reporter Ai65<sup>10</sup> (Jax stock# 021875) to obtain selective labeling of  
942 Lamp5/Lhx6 cells. Tamoxifen (20 mg/ml in corn oil) was administered to *Id2-CreER; Nkx2.1-Flpo;*  
943 *Ai65* animals (3 × 5 mg by oral gavage over 5 days) between P30–P40 to activate the CreER,  
944 after which animals were either perfused with 4% PFA/PBS and their brains processed for  
945 immunohistochemistry (20- $\mu$ m cryosections; tdTomato signal was enhanced using rabbit anti-  
946 RFP from Rockland Immunochemicals; cat# 600-401-379), or acute brain slices were prepared  
947 for morphological fills as described previously<sup>11</sup>. Fluorescence images were acquired on a Zeiss  
948 Axio Imager.A1 and levels/contrast adjustments performed using Photoshop (Adobe).

949

### 950 **Ferret 10X Chromium Single Cell 3' v3**

951 A dataset of 801 interneurons was generated from ferret (P42) striatum. Single-nuclei  
952 suspensions from frozen tissue was generated as for Drop-seq; GEM generation and library  
953 preparation followed protocol #CG000183\_ChromiumSingleCell3'\_v3\_UG\_Rev-A. Sequencing,  
954 alignment and clustering (using the ICA pipeline described above) proceeded as for the Drop-seq  
955 datasets above.

956

957 **METHODS REFERENCES**

958

- 959 1. Saunders, A. *et al.* Molecular Diversity and Specializations among the Cells of the  
960 Adult Mouse Brain. *Cell* **174**, 1015–1030 (2018).
- 961 2. Paxinos, G., Watson, C., Petrides, M., Rosa, M. & Tokuno, H. *The marmoset brain*  
962 *in stereotaxic coordinates*. (2012).
- 963 3. Macosko, E. Z. *et al.* Highly Parallel Genome-wide Expression Profiling of Individual  
964 Cells Using Nanoliter Droplets. *Cell* **161**, 1202–1214 (2015).
- 965 4. Welch, J., Kozareva, V., Ferreira, A., bioRxiv, C. V.2018. Integrative inference of  
966 brain cell similarities and differences from single-cell genomics. *bioRxiv.org*  
967 doi:10.1101/459891
- 968 5. Hodge, R. D. *et al.* Conserved cell types with divergent features between human  
969 and mouse cortex. *bioRxiv.org*  
970 (2018). doi:10.1101/384826
- 971 6. Lek, M. *et al.* Analysis of protein-coding genetic variation in 60,706 humans. *Nature*  
972 **536**, 285–291 (2016).
- 973 7. Mayer, C. *et al.* Developmental diversification of cortical inhibitory interneurons.  
974 *Nature* **555**, 457–462 (2018).
- 975 8. Rawlins, E. L., Clark, C. P., Xue, Y. & Hogan, B. L. M. The Id2+ distal tip lung  
976 epithelium contains individual multipotent embryonic progenitor cells. *Development*  
977 **136**, 3741–3745 (2009).
- 978 9. He, M. *et al.* Strategies and Tools for Combinatorial Targeting of GABAergic  
979 Neurons in Mouse Cerebral Cortex. *Neuron* **91**, 1228–1243 (2016).
- 980 10. Madisen, L. *et al.* Transgenic mice for intersectional targeting of neural sensors and  
981 effectors with high specificity and performance. *Neuron* **85**, 942–958 (2015).
- 982 11. Schuman, B. *et al.* Four Unique Interneuron Populations Reside in Neocortical  
983 Layer 1. *J. Neurosci.* **39**, 125–139 (2019).

984

985